Ore Geology Reviews 56 (2014) 352–372

Contents lists available at ScienceDirect

Ore Geology Reviews

journal homepage: www.elsevier.com/locate/oregeorev

Review

Geology and geochemistry of Middle Eocene Maden complex ferromanganese deposits from the Elazığ–Malatya region, eastern Turkey

Ahmet Şaşmaz [a,*], Bayram Türkyilmaz [b], Nevin Öztürk [a], Fuat Yavuz [c], Mustafa Kumral [c]

[a] Department of Geological Engineering, Fırat University, Elazığ 23119, Turkey
[b] General Directorate of Mineral Research and Exploration, Malatya 44040, Turkey
[c] Department of Geological Engineering, Istanbul Technical University, 34469 Maslak, Istanbul, Turkey

ARTICLE INFO

Article history:
Received 9 May 2012
Received in revised form 20 June 2013
Accepted 20 June 2013
Available online 3 July 2013

Keywords:
Mn–Fe deposits
REE chemistry
Elazığ–Malatya
Turkey

ABSTRACT

In the study region, the Pütürge Precambrian–Permian metamorphic rocks, the Upper Jurassic–Lower Cretaceous Guleman ophiolites, the Upper Cretaceous–Lower Eocene Hazar unit, the Campanian–Lower Maastrichtian aged Elazığ magmatics, and the Middle Eocene Maden complex crop out extensively. The Maden complex containing ferromanganese mineralization unconformably overlies the Pütürge metamorphic rocks, the Guleman ophiolites, and the Hazar unit and is unconformably overlain by Plio–Quaternary sediments. The ferromanganese (Mn–Fe) ores in the Elazığ–Malatya region, eastern Turkey, are hosted in the mudstone member of the volcano-sedimentary part of the Middle Eocene Maden complex as lenses or interbedded layers. In the Elazığ–Malatya region, Mn–Fe ores occur at eight localities, namely, Beyhan, Palu, Sarıkamış, Koçkale, Germili, Hazar, Alihan, and Kom. Mn–Fe ores are found in the Koçkale and Palu deposits as a single bed but in the Hazar and Kom deposits as two beds and in the Sarıkamış, Germili, and Alihan deposits in three levels. The thickness of these mineralized levels ranges from 0.3 m to 10 m. All the investigated mineralizations are conformable with the foot wall mudstones. Braunite, bixbyite, jacobsite, pyrolusite, manganite, and psilomelane are the main manganese oxide minerals. Hematite, barite, and pyrite are also found in variable amounts in the ferromanganese ores. The trace element content of all studied ferromanganese deposits is generally in low concentrations and tends to enrichment in the assemblage of Ba, Sr, V, Cu, Pb, Zn, and As with a geochemical characteristic similar to hydrothermal deposits. Rare earth element (REE) patterns of the Maden complex Mn–Fe deposits support a hydrothermal origin, with a slight enrichment in the middle REE (4.04–29.91 ppm, average = 16.49) and a slightly high concentration of total REE (92.40–738.23 ppm, average = 517.85). In all the investigated deposits, REE patterns displayed negative Ce (0.08 to 0.72, average = 0.15) and Eu (0.55 to 0.82, average = 0.72) anomalies. This shows that low-temperature hydrothermal fluids played an important role in the formation of mineralization. The ore deposition is similar to that of sedimentary-exhalative mineralization, deposited within the Maden marginal basin.

Contents

* Corresponding author.
E-mail address: asasmaz@firat.edu.tr (A. Şaşmaz).

0169-1368/$ – see front matter © 2013 Elsevier B.V. All rights reserved.
http://dx.doi.org/10.1016/j.oregeorev.2013.06.012

1. Introduction

Manganese deposits can be formed by various processes, including sedimentary, hydrothermal, hydrogenous, and supergene. Hydrothermal manganese deposits are smaller than sedimentary manganese deposits (Roy, 1992). Hydrothermal manganese ores are precipitated from low-temperature hydrothermal solutions and are generally stratabound or occur as irregular bodies and epithermal veins. They are formed in different tectonic settings, such as the marine environment next to spreading centers, intraplate seamounts, or in subduction-related island arc settings, and are found in both modern and ancient geologic environments (Roy, 1997).

Manganese and ferromanganese ore deposits are recognized in different ages and geologic settings in Turkey (Öztürk, 1993). For example, the Lower Cretaceous Denizli–Tavas–Ulukent (southwest Turkey) Mn ore deposit has a diagenetic genesis (Kuşçu and Gedikoğlu, 1989); the Upper Cretaceous Ankara–Çayırlı (central Turkey) Mn deposit (Oygür, 1990), Adıyaman–Koçali (southeast Turkey) Mn deposit (Öztürk, 1993), and Middle Eocene Elazığ–Koçkale (east Turkey) Mn and Mn–Fe deposits (Altunbey and Sağıroğlu, 1995) have a volcano-exhalative genesis; the Upper Cretaceous Trabzon–Ocaklı (northeast Turkey) Mn deposit has a hydrothermal genesis (Gedikoğlu et al., 1985). Although volcano-sedimentary rocks and their associated Mn–Fe deposits in the Elazığ–Malatya region are widely distributed, studies focused on their geologic, mineralogical, and geochemical characteristics are limited.

The Mn–Fe ores in the Elazığ–Malatya region (Fig. 1A), eastern Turkey, are found in the Maden complex, a volcano-sedimentary formation of Middle Eocene age. The Mn–Fe mineralization mostly occurs as lenses and stratiform layers, which are restricted to the Maden marginal basin. This basin and associated structures are associated with stages of the Neotethyan evolution (Aktaş and Robertson, 1984, 1990; Elmas and Yılmaz, 2003; Michard et al., 1984; Rızaoğlu et al., 2006; Robertson et al., 2007; Yazgan and Chessex, 1991; Yiğitbaş and Yılmaz, 1996a). The recognized ore minerals are braunite, bixbyite, jacobsite, pyrolusite, manganite, psilomelane, hematite, barite, and pyrite.

The Maden complex also hosts the Ergani (Maden) copper deposit, which has mineralized sections that are recognized over an area of 200 km^2 (Bamba, 1976). The spatial relationship between copper and ferromanganese mineralization has not been researched in detail, even though both types of mineralization are hosted by the same volcano-sedimentary formation.

There has been no detailed investigation on the origin of the Mn–Fe mineralization from the Elazığ–Malatya region. In contrast, the genesis of the Ergani (Maden) copper deposit is clear, and an exhalative sedimentary model has been proposed to explain its origin (Bamba, 1976; Borchert, 1952; Erdoğan, 1977; Erler, 1983; Göymen and Aslaner, 1969; İleri et al., 1976; Schneiderhöhn, 1954; Sirel, 1949). The purpose of this paper is to discuss new field observations in conjunction with major, trace, and rare-earth element (REE) geochemical data to constrain the genesis of Mn–Fe ore deposits in the Elazığ–Malatya region, eastern Turkey.

2. Tectonic evolution of the region

Turkey (Anatolia) was located at the boundary between the Gondwana and Laurasia continents to the south and north, respectively. Anatolia was formed from several oceanic and continental crusts as a result of numerous continental fragments rifting off from the main body and joining the next fragment. The present distribution of Anatolian terranes is controlled by Alpine orogeny (Göncüoğlu et al., 1997).

The neotectonic evolution of Turkey is controlled by the collision of the African and Arabian plates with the Eurasian plate along the Hellenic (Aegean) arc, and the Bitlis–Zagros suture zone (Elitok and Dolmaz, 2011). The Bitlis–Zagros suture zone extends to the Alpine–Appenine mountain belt and the Owen transform fault. The collision of the African and Eurasian plates resulted in the North Anatolian fault (NAFZ; dextral strike slip) and the East Anatolian fault (EAFZ; sinistral strike slip). The Anatolian plate has escaped westwards since then (Akıncı, 2009; Bozkurt, 2001) (Fig. 1B).

The southern Neotethys was opened during the Triassic as a result of rifting of one or several microcontinents from Gondwana; these microcontinents then spread northwards (Robertson and Dixon, 1984; Robertson et al., 2007; Şengör and Yılmaz, 1981). The evolution of the southern Neotethys Ocean is important in explaining the close association of the Maden complex and the Mn–Fe deposits. The south Neotethyan suture zone exposed in the Elazığ–Malatya region was investigated with respect to five main tectonic stages by Robertson et al. (2007): (1) Middle–Late Triassic rifting and spreading of the southern Neotethys; the southern ocean began opening during the Late Triassic (Fig. 2A); (2) Late Cretaceous northward subduction–accretion of ophiolites and arc-related units (Fig. 2B and C); (3) Middle Eocene subduction-related extension (Fig. 2D); (4) Early–Middle–Miocene collision and southward thrusting over the Arabian Foreland (Fig. 2E); and (5) Plio–Quaternary, post-collisional left-lateral tectonic escape. After the formation and emplacement of ophiolites during the Late Cretaceous, a large, fault-bounded, extensional basin, namely the Maden marginal basin, was formed by northward subduction during the Middle Eocene (Robertson et al., 2007). The Maden basin was infilled with shallow- to deep-water sediments and subduction-related volcanic rocks, which host the Mn–Fe deposits.

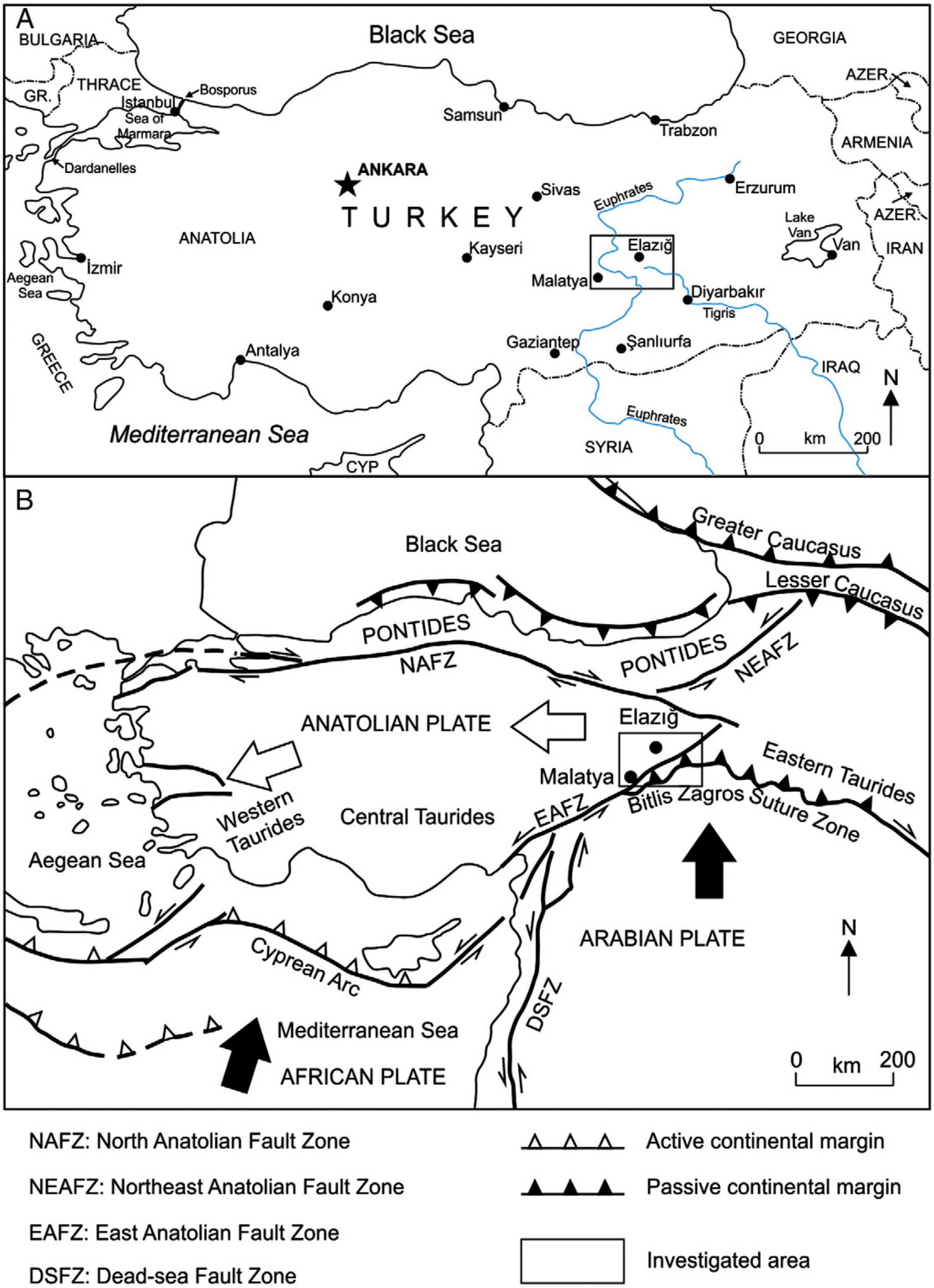

Fig. 1. Simplified tectonic map of Turkey showing major tectonic structures and plates and location of the study area (simplified and modified from Gürbüz and Gül, 2005). DSFZ = Dead-Sea Fault Zone, NEAFZ = Northeast Anatolian Fault Zone, EAFZ = East Anatolian Fault Zone, and NAFZ = North Anatolian Fault Zone.

3. Geologic setting

The Maden basin, in which the Middle Eocene Maden complex was formed, hosts the Mn–Fe deposits of the Elazığ–Malatya region (e.g., Beyhan, Palu, Sarıkamış, Koçkale, Germili, Hazar, Alihan, and Kom; Fig. 3) and is bound to the north–northwest by Cretaceous ophiolites, Late Cretaceous magmatic rocks, Cretaceous–Pliocene-covered sedimentary rocks, Plio–Quaternary sediments, and metamorphic complexes; Cretaceous–Pliocene cover sedimentary rocks to the south–southwest and southeast, respectively (Fig. 3).

The oldest rocks in the Elazığ–Malatya region are Precambrian–Devonian high-grade metamorphic rocks (augen gneisses, amphibolites, mica schists/gneisses, granitic gneisses), Carboniferous–Permian low-grade metamorphic rocks (calc-schists/marbles and schists) (i.e., the Pütürge metamorphics), Upper Jurassic–Lower Cretaceous ophiolitic rocks (peridodite, banded gabbro, pillow basalt) (i.e., the

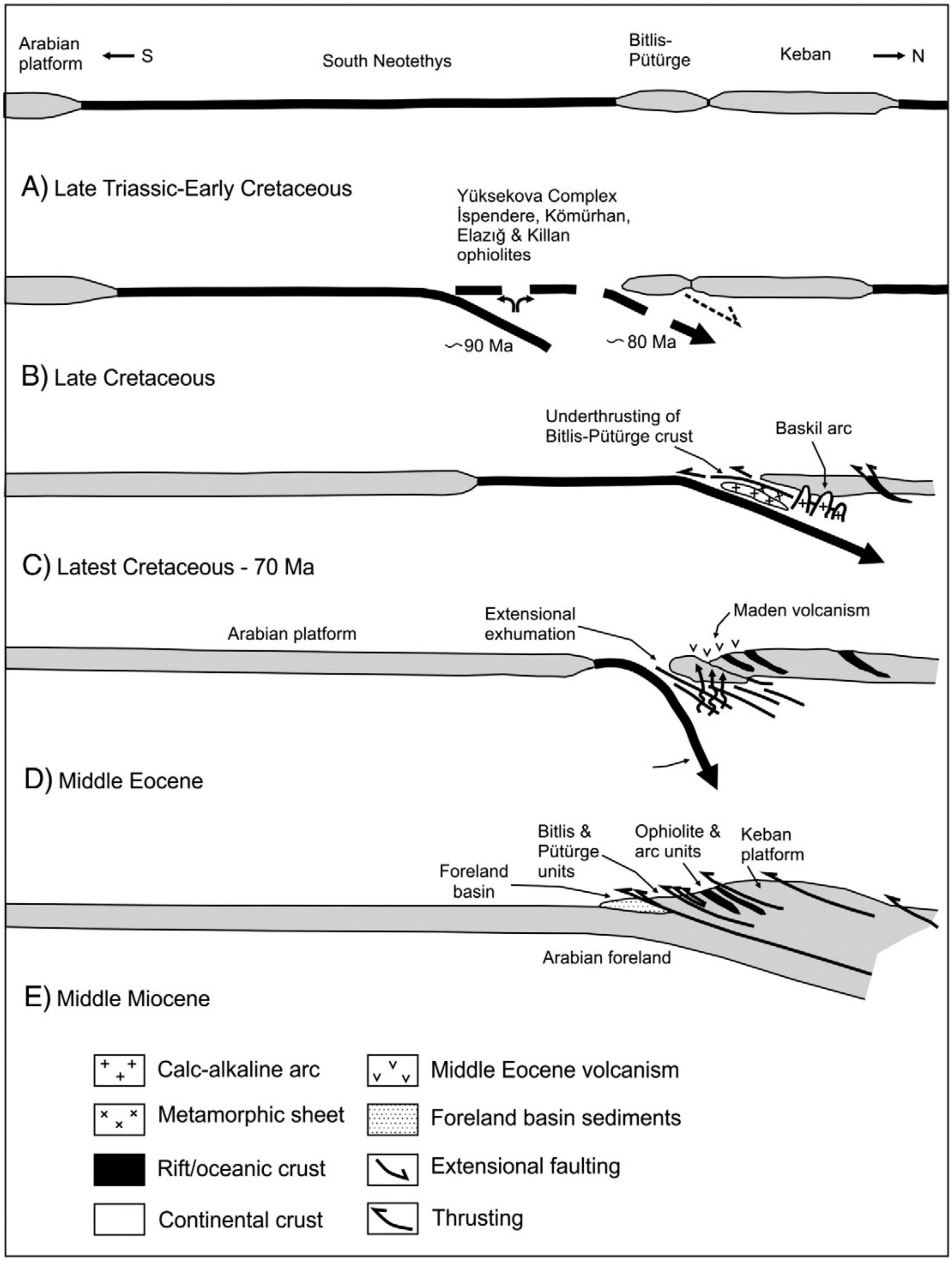

Fig. 2. Tectonic evolution of the Tauride thrust belt in SE Turkey.
Taken from Robertson et al. (2007).

Guleman ophiolite), and Upper Cretaceous–Lower Eocene sedimentary rocks (mudstone, sandstone–mudstone–marl, limestone) (i.e., the Hazar unit). Gneisses and mica schists of the Pütürge metamorphics have been dated as 505 ± 37 and 596 ± 88 Ma, respectively, using K–Ar geochronology (Yılmaz, 1971). These metamorphic, ophiolitic, and sedimentary rocks represent the basement of the Maden basin (Erdoğan, 1982; Yazgan, 1981, 1984). The Pütürge metamorphic rocks crop out around the Pütürge (Malatya) district, 73 km southeast of the town of Malatya, between the Çelikhan (Adıyaman) and Sivrice (Elazığ) districts. The Guleman ophiolitic rocks crop out around the Maden (Elazığ) district, 78 km southeast of the town of Elazığ. The Hazar unit sedimentary rocks crop out around Hazar Lake, 22 km northeast of the town of Elazığ.

The Maden complex lies unconformably over the Pütürge metamorphic, the Guleman ophiolitic, and the Hazar unit sedimentary rocks (Fig. 4) (Kaya, 2004; Robertson, 2000; Yazgan, 1984; Yiğitbaş and Yılmaz, 1996a, 1996b; Yılmaz and Yiğitbaş, 1990). The Campanian–Lower Maastrichtian Elazığ magmatic rocks (Hempton and Savcı, 1982) and the Guleman ophiolites are tectonically juxtaposed over the Maden complex. Elazığ magmatic rocks comprise plutonic (diorite, tonalite, granodiorite), volcanic (basalt, andesite), and volcano-sedimentary (andesitic pyroclastic) rocks. Guleman ophiolites are composed of peridotite,

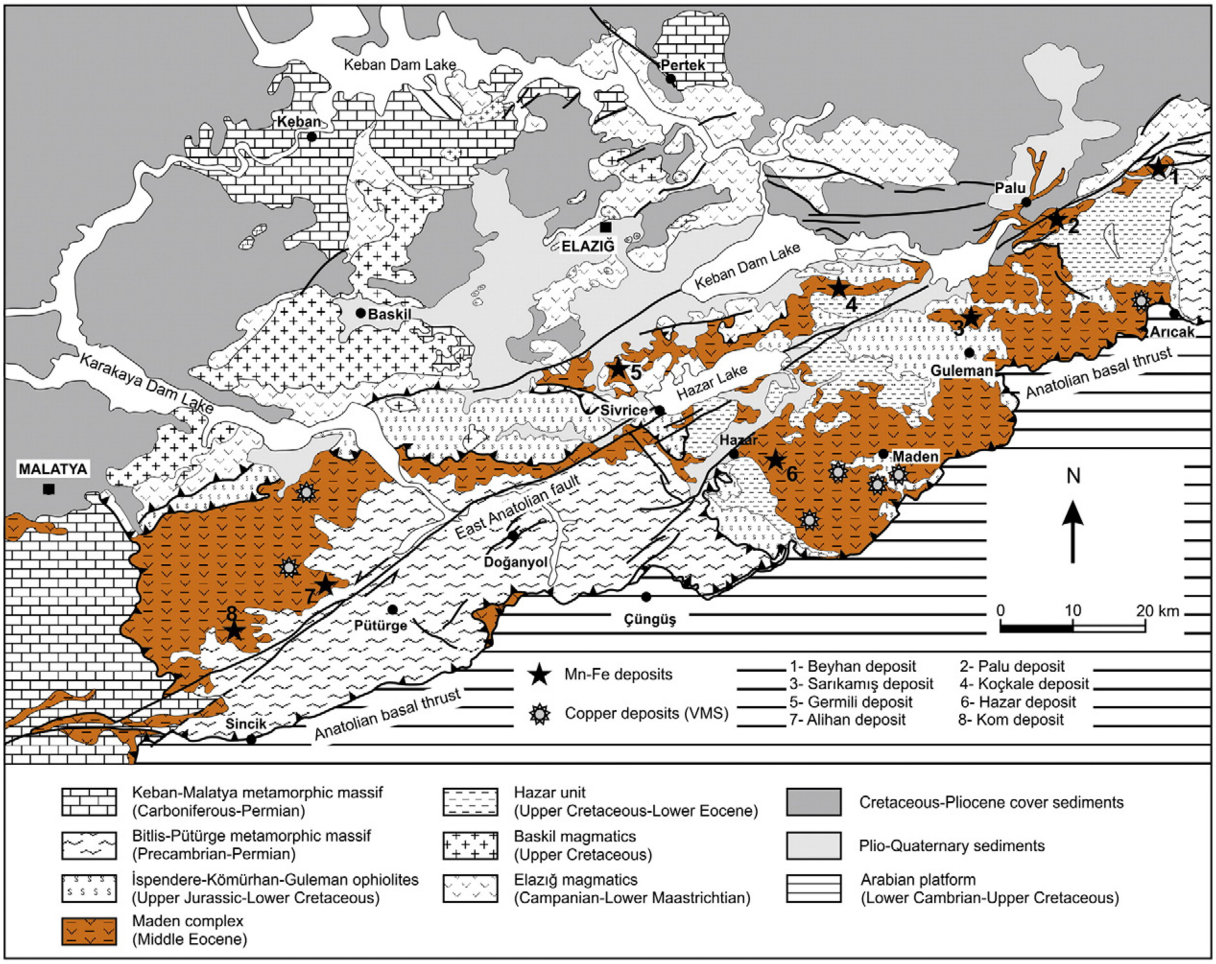

Fig. 3. Regional geological map of the Elazığ-Malatya region.
Taken from Mineral Research and Exploration, MTA (2002).

gabbro, troctolite, diabase dykes, basaltic lavas, and micritic limestones. Plio–Quaternary sedimentary rocks cover all the older units.

3.1. The Maden complex

The Maden complex is the most important unit in the Elazığ–Malatya region in terms of a close association with Mn–Fe mineralization. The unit hosts the Mn–Fe oxide deposits of the Elazığ–Malatya region (e.g., Beyhan, Palu, Sarıkamış, Koçkale, Germili, Hazar, Alihan, Kom; Fig. 3) and crops out over large areas between the Maden (Elazığ)–Pütürge (Malatya) region; it is transgressed by Eocene sediments. Geologic, petrographical, and geochemical properties of the Maden complex have been previously investigated by Açıkbaş and Baştuğ (1975), Perinçek (1978), Aktaş and Robertson (1984), Yazgan (1984), Özçelik (1985), Yazgan et al. (1986, 1987), Yıldırım and Yılmaz (1991), Yiğitbaş et al. (1993), Turan et al. (1995), Yiğitbaş and Yılmaz (1996a), and Robertson et al. (2007). Among these investigations, Perinçek (1978) identified *Globorotalia bullbrooki*, *Truncorotaloides topilensis*, *Globorotalia* sp., *Globigerina* sp., *Nummulites* sp., *Nummulites millecaput*, *Nummulites* cf. *aturicus*, *Discocycline* sp., *Sfhaerogypsina* sp., and *Assilina* sp. fossils, leading to a determination of the Middle Eocene age. Yazgan (1984) obtained 48 Ma for the Maden complex using K–Ar geochronology.

The Maden complex unconformably overlies the Guleman ophiolites around the town of Maden (Elazığ), the Hazar unit east of Hazar Lake, and the Pütürge metamorphics around the town of Pütürge (Malatya) (Figs. 3 and 4). The Guleman ophiolites and Elazığ magmatics lie tectonically over the Maden complex. The thickness of the Maden complex varies from 100 to 750 m (Açıkbaş and Baştuğ, 1975). The Maden complex volcano-sedimentary units have been divided into four formations by Açıkbaş and Baştuğ (1975): the Ceffan formation (basal conglomerate, sandstone, sandy limestone), the Arbo formation (sandy–clayey limestone–tuffite–neritic limestone), the Melafan formation (pelagic limestone, mudstone, spilitic lavas, radiolarite, chert), and the Karadere formation (altered basalt and andesite).

3.1.1. Ceffan formation

The Ceffan formation unconformably overlies the Pütürge metamorphics, the Guleman ophiolites, and the Hazar unit and is conformably overlain by the Arbo formation (Fig. 4). The formation begins with a green-colored basal conglomerate. Basal conglomerates are composed of subrounded–rounded boulders and pebbles derived from the Pütürge metamorphic and Guleman ophiolitic rocks (Erdoğan, 1982; Yazgan et al., 1987). The sequence continues with medium- to thin-bedded sandstones. The upper part of the unit is represented by sandy limestone and shale intercalations.

3.1.2. Arbo formation

The Arbo formation conformably overlies the Ceffan formation sedimentary rocks and is conformably overlain by the Melafan formation (Fig. 4), which is composed of limestone with abundant nummulite fossils. The upper part of the formation contains rhyolite and tuff (Robertson et al., 2007). Neritic limestones are found in the uppermost level of the formation.

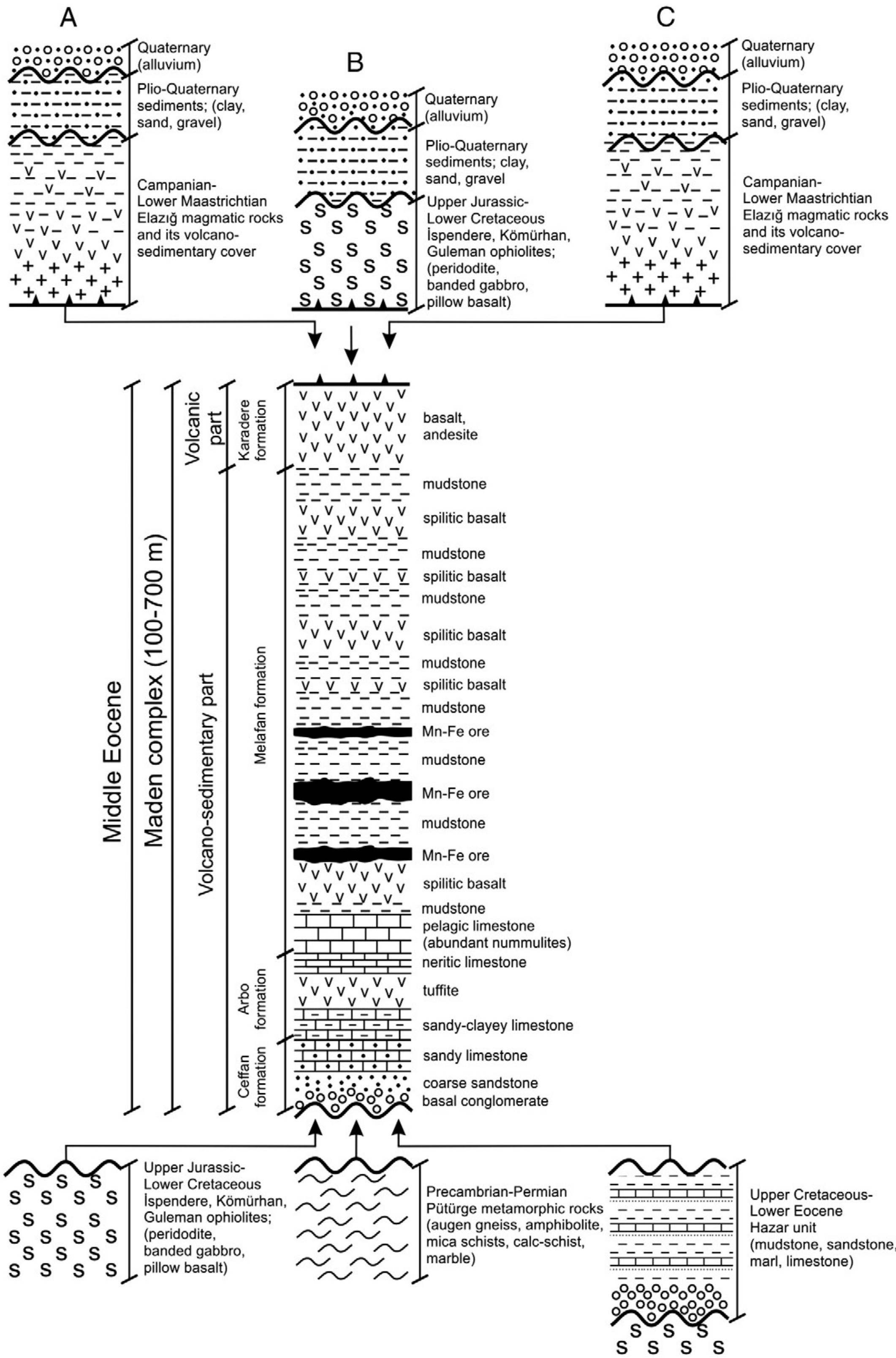

Fig. 4. Generalized stratigraphic column showing the relations of the Maden complex with (A) Guleman ophiolites, (B) Pütürge metamorphics, and (C) Hazar unit. Modified and simplified from Erdoğan (1982), Yazgan and Chessex (1991), Gürocak (1992), Kaya (2004), Robertson et al. (2007), and Nurlu (2009).

3.1.3. Melafan formation

The Melafan formation conformably overlies the Arbo formation and is conformably overlain by the Karadere formation (Fig. 4). The sequence begins with pelagic limestones, which are overlain by intercalated radiolarite, chert, and spilitic lavas (Bozkaya et al., 2006). Reddish-colored mudstones, in places, either interfinger with spilitic volcanics or overlie these rocks. In this study, we recognized that the Mn–Fe deposits are located in the Melafan formation when this formation lies directly on spilitic lavas or is interbedded with reddish mudstones.

3.1.4. Karadere formation

The Karadere formation conformably overlies the Melafan formation and is tectonically overlain by Elazığ magmatics and Guleman ophiolites (Fig. 4); it comprises black-colored basalts and andesites. The formation also contains pyroclastics (agglomerate, lapillistone, tuff) and subvolcanic rocks (diabase, microgabbro, microdiorite, microsyenite) (Yazgan et al., 1987).

The Middle Eocene Maden complex is interpreted as an immature island arc (Erdoğan, 1977), an intra-crustal subduction (Michard et al., 1985; Yazgan, 1983, 1984), a back-arc basin (Hempton, 1984, 1985; Şengör and Yılmaz, 1981), or an immature back-arc basin (Yiğitbaş and Yılmaz, 1996a, 1996b). Coarse-grained sediments found in the Ceffan formation indicate deposition in terrestrial or a shallow marine environment. The release of coarse-grained particles and the formation of clastic rocks are caused by compression and uplift along the basin margins (Robertson et al., 2007). Although the lower section of the Arbo formation is deposited in a shallow marine environment, the upper part is deposited in a deeper environment. Siliceous tuffs in the middle section of the unit indicate that volcanism occurred in shallow water or on land (Robertson et al., 2007). The Melafan formation shows deep marine features. This unit reflects transgressive depositional characteristics in a rapidly deepening environment. The lower part of the formation consists of clastic rocks derived from metamorphic rocks. With increasing depth this sequence passes into carbonate rocks and fine-grained clastic and siliceous chemical rocks. Radiolarite and chert (siliceous sediments) occur below the carbonate compensation depth (CCD). Later, basaltic and andesitic lavas were spread on the sea floor and caused the development of spilitic pillow lavas (Roberson et al., 2007).

The volcanic rocks of the Maden complex are classified as basalt, andesite, and minor dacite based on immobile trace element concentrations in the Poluşağı (Pütürge–Malatya) area (Özçelik, 1985). According to Özçelik (1985), immobile trace and some major element chemistry of the Maden complex magmatic rocks demonstrates a typical tholeiitic character; the Maden complex tholeiitic basalts exhibit chemical characteristics of oceanic tholeiites and island arc tholeiites. From geochemical and geologic considerations, Özçelik (1985) concluded that the Maden complex rock suite was produced during the initial stages of an ensimatic immature island arc volcanism, which developed on the oceanic crust of the Middle Eocene Maden marginal basin. Yazgan (1981) concluded that the volcanic rocks of the Maden complex have a tholeiitic to calc-alkaline character based on geochemical data. Bozkaya et al. (2006) concluded that the rocks of the Maden complex metamorphosed under greenschist facies conditions (approximately 200–300 °C and 2–3 kbar). Robertson et al. (2007) indicated that the Maden complex was affected by overthrusting, which gave rise to greenschist metamorphism. This kind of metamorphism is characteristic of back-arc basins (Bozkaya et al., 2006) and supports the interpretation of a back-arc basin (Bozkaya et al., 2006; Hempton, 1984; Önal and Bingöl, 1997; Perinçek and Özkaya, 1981; Yiğitbaş and Yılmaz, 1996a; Yılmaz, 1993, 1999) for the formation of the Maden complex.

3.2. Fe–Mn deposits

Numerous studies (Açıkbaş and Baştuğ, 1975; Özkaya, 1974, 1978; Perinçek, 1978; Rigo de Righi and Cortesini, 1964; Sungurlu, 1975) have focused on the volcano-sedimentary units of the Elazığ–Malatya region and surrounding areas. Helke (1938) first recognized Mn–Fe mineralization of the region, and since then several investigations (Altunbey and Sağıroğlu, 1995; Bamba, 1973; Karaman et. al., 1993; Ketin, 1948; Kovenko, 1943, 1944; Mohr, 1964; Önal et al., 2001; Türkyılmaz, 2004; Yazgan, 1972; Yazgan et. al., 1987) have described these Mn–Fe deposits in some detail; however, information on the specific properties of the ore deposits remains limited. In addition several studies have focused on the Ergani (Maden) copper deposit (Bamba and Tin, 1972; Borchert, 1952; Göymen and Aslaner, 1969; Griffits et. al., 1972; Helke, 1961; Sirel, 1952; Takashima, 1975; Wijkerslooth, 1943, 1944). In this paper, we provide a brief description of the Mn–Fe deposits of the Elazığ–Malatya region based on our field studies.

3.2.1. Beyhan deposit

The Beyhan deposit is located 4 km west of the town of Beyhan (Fig. 3); Mn–Fe ore outcrops are spread out over a large area. In the Beyhan deposit area, the ore-bearing volcano-sedimentary part of the Maden complex has an unconformable lower contact with the Hazar unit and an unconformable contact with the overlying Plio–Quaternary sediments (Fig. 5A). The ore-bearing formation comprises spilitic volcanics, mudstones, and radiolarites. The ore bodies are conformable with the host rock and occur as three lenticular horizons within reddish mudstones of the volcano-sedimentary section of the Maden complex. The lowermost lens is 1.5 to 2.5 m thick and lies directly on the spilitic basalt. The central lens is separated from the lower by 5 m of mudstone, varying in thickness from 1 to 1.5 m. The uppermost lens lies 7 m above the central layer, varying in thickness from 40 to 60 cm. The ores trend approximately northwest–southeast and dip northeast between 30° and 70°. The lengths of the ore lenses vary from 500 to 600 m. The lower volcano-sedimentary section of the Maden sequence is overlain by an upper subunit of basalt and andesite.

3.2.2. Palu deposit

The Palu deposit is located around Yeşilbayır village, 2 km south of the town of Palu (Fig. 3). In the Palu deposit area, the Mn–Fe ore-bearing volcano-sedimentary part of the Maden complex has an unconformable lower contact with the Hazar unit and an unconformable contact with the overlying Plio–Quaternary sediments (Fig. 5B). There is only one orebody, which is lenticular in shape and comformable with the host rock. The orebody lies approximately 6 m above the spilitic basalt–mudstone contact and is completely hosted within mudstone and in places interlinks with the mudstone. The ore lense generally varies in thickness from 2 to 3 m and in length from 30 to 50 m. Spilitic basalt–ore–mudstone intercalations are overlain by basalt and andesites. Some ore was removed by short-term mining operations at Palu, but such operations stopped in 2009.

3.2.3. Sarıkamış deposit

The Sarıkamış deposit is located 500 m northeast of Sarıkamış village (Fig. 3). In the Palu deposit area, the Mn–Fe ore-bearing volcano-sedimentary part of the Maden complex has an uncomformable lower contact with the Guleman ophiolite and an uncomformable contact with the overlying Plio–Quaternary sediments (Fig. 5C). The orebodies trend approximately northwest. Three Mn–Fe orebodies are lenticular in shape and occur interstratified with mudstone, which shows a lateral change in color from reddish-brown to black. The first orebody lies directly on the radiolarites. The thickness of the first orebody varies between 0.5 and 3 m. The second orebody (from the bottom) is completely hosted in mudstone, and the thickness of this lens varies between 50 and 60 cm. The topmost orebody (third orebody) is thinner (30–40 cm) and laterally impersistent. The total ore zone thickness varies from 14 to 15 m. Ore has been exploited mainly by small-scale miners using rudimentary methods at Sarıkamış.

3.2.4. Koçkale deposit

The Koçkale deposit is the most important source of manganese in the Elazığ–Malatya region and is located between the villages of Koçkale and Genefik, 24 km east of Elazığ (Fig. 3). The Koçkale deposit has a reserve of 1970 kt with grades of 29% Fe, 17% Mn, and 13% Si (Altunbey and Sağıroğlu, 1995). In the Koçkale deposit area, the Mn–Fe ore-bearing volcano-sedimentary part of the Maden complex has an uncomformable lower contact with the Hazar unit and an uncomformable contact with the overlying Plio–Quaternary sediments

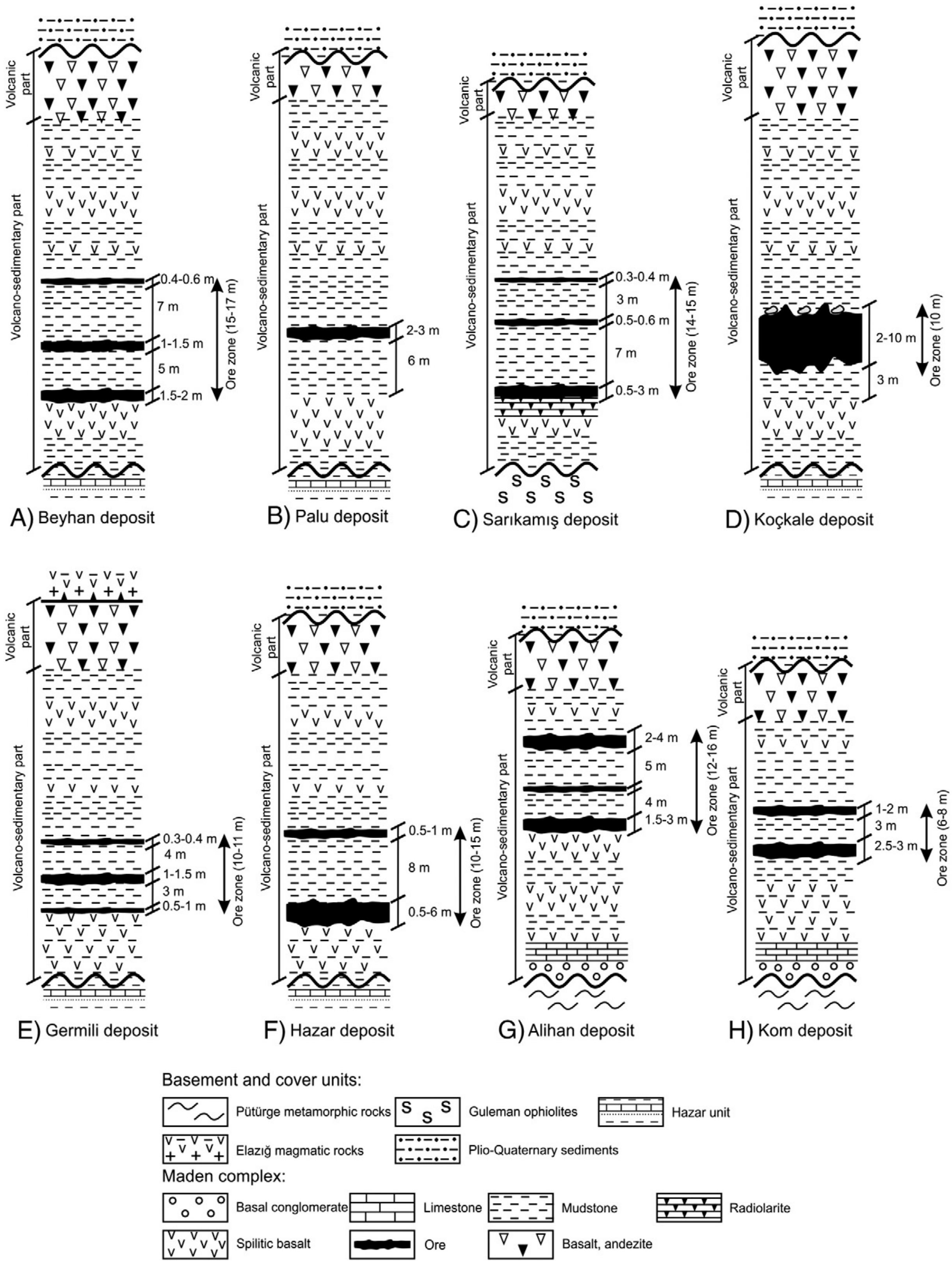

Fig. 5. Stratigraphic columns of the Mn–Fe deposits of the Elazig–Malatya region, east Turkey.

(Fig. 5D). The ore bodies are lenticular in shape but comformable with the host rock and occur as one lenticular body completely within reddish mudstones. The ore lens lies 3 m above the spilitic basalt–mudstone contact, varying in thickness from 2 to 10 m and lengths from 1 to 4 km. The ore trends approximately northwest–southeast and dips southeast between 25° and 35°. This manganese oxide lens is crosscut by silica veins. Yellowish-white barite lenses are observed within an upper section of the ore. The thickness of the sulfur zone ranges from 0.5 to 2 m and alters to limonite. Spilitic basalt–ore–mudstone intercalations are overlain by basalt and andesite. Diabase and spilitic basalt are found extensively in the lower part of the Maden volcano-sedimentary complex and include manganese oxides within the fracture and fissure zones. However, manganese mineralization was encountered within the fracture and fissure zones of basalt and andesite (i.e., Karadere formation) that overlie the volcano-sedimentary sequence, and in the upper part of the Maden complex. Epigenetic ferromanganese veins belonging to the Maden complex and located within fractures and cracks of mudstones are observed only in this deposit. The thickness and length of these veins range from 0.5 to 4 m and 5 to 60 m, respectively (Altunbey and Sağıroğlu, 1995). According to Altunbey and Sağıroğlu (1995), epigenetic ferromanganese veins show mineralogical and textural features similar to those of syngenetic occurrence, suggesting that mineralization formed due to the channels that feed them.

3.2.5. Germili deposit

The Germili deposit is located 18 km southeast of Elazığ on the Elazığ–Sivrice highway just left of the Kinederiş ramp (Fig. 3). The Upper Cretaceous Elazığ magmatics and its volcano-sedimentary cover widely outcrop in the area. In the Germili deposit area, the Mn–Fe ore-bearing volcano-sedimentary part of the Maden complex has an uncomformable lower contact with the Hazar unit and a tectonic contact with the overlying Elazığ magmatic rocks (Fig. 5E). The ore bodies are comformable with the host rock and occur as three lenticular bodies within reddish mudstones. The lowermost lens is 0.5 to 1 m thick and lies directly on the spilitic basalt. The central lens is separated from the lower by 3 m of mudstone, varying in thickness from 1 to 1.5 m. The uppermost lens lies 4 m above the central layer, varying in thickness from 30 to 40 cm. The ores trend approximately east–west and dip north between 70° and 80°. The lengths of the ore lenses vary from 350 to 400 m. Spilitic basalt–ore–mudstone intercalations are overlain by basalt and andesite.

3.2.6. Hazar deposit

The Hazar deposit is located 2 km southeast of Hazar village (Fig. 3). In the Hazar deposit area, the Mn–Fe ore-bearing volcano-sedimentary part of the Maden complex has an uncomformable lower contact with the Hazar unit and an uncomformable contact with the overlying Plio–Quaternary sediments (Fig. 5F). Hazar mineralizations are observed at three distinct areas: the Toplu hill, the Katran hill, and the Mezarlık hill. However, there are many other large and small occurrences that show the same characteristics as the main mineralizations. The Toplu hill mineralization outcrops occur in the valley to the south of Toplu hill and lie in a northeast–southwest direction along the Bektaş and Tilkitaş ridge. The thickness of this lens varies from 0.5 to 6 m, and the length is 1400–1500 m. The ore bodies are lenticular in shape but comformable with the host rock and are hosted within reddish mudstones. The lower lens is 0.5 to 6 m thick and lies directly on the spilitic basalt. The upper lens is separated from the lower by 8 m of mudstone, varying in thickness from 0.5 to 1 m. The ores trend approximately northwest–southeast and dip north between 50° and 60°. The lengths of the ore lenses vary from 1400 to 1500 m. The Katran hill mineralization outcrops occur southwest of Katran hill. The ore lens occurs either within mudstones or along the contact of the mudstone–spilitic basalt. Ore thicknesses vary from 0.5 to 1.5 m and lengths are 200–250 m. The Mezarlık hill mineralization outcrops on a ridge between Mezarlık and Taşlık hills. The ore lens is entirely hosted within mudstones with thicknesses varying from 8 to 10 cm, and lengths of 150–200 m. Spilitic basalt–ore–mudstone intercalations are overlain by basalt and andesite.

3.2.7. Alihan deposit

The Alihan deposit is the second most important source of manganese in the Elazığ–Malatya region and is located near the Alihan village, 70 km southeast of Malatya (Fig. 3). The Alihan deposit has a reserve of 320 kt with grades of 35% Fe_2O_3, 19% MnO, and 23% SiO_2 (Önal et al., 2001). Production of 20 kt has been recorded from the Alihan mine and is ongoing. In the Alihan deposit area, the Mn–Fe ore-bearing volcano-sedimentary part of the Maden complex has an angular uncomformable lower contact with the Pütürge metamorphics and an uncomformable contact with the overlying Plio–Quaternary sediments (Fig. 5G). The ore bodies occur as three lenticular bodies hosted in reddish mudstones with the lowermost lens being 1.5 to 3 m thick and lying directly on the spilitic basalt. The central lens is separated from the lower one by 4 m of mudstone, varying in thickness from 1.5 to 2 m whereas the uppermost lens lies 5 m above the central layer, varying in thickness from 2 to 4 m. The ores trend approximately east–west and dip north between 20° and 50° having lengths from 450 to 500 m, 80 to100 m, and 130 to150 m, respectively. Spilitic basalt–ore–mudstone intercalations are overlain by basalt and andesite. Most of the ore bodies have been exploited and only low-grade ores are left.

3.2.8. Kom deposit

The Kom deposit is located 40 km southeast of Malatya, 3 km southwest of Pütürge, and 1.5 km northeast of the Destişur hill (Fig. 3). In the Kom deposit area, the Mn–Fe ore-bearing volcano-sedimentary part of the Maden complex has an angular uncomformable lower contact with the Pütürge metamorphics and an uncomformable contact with the overlying Plio–Quaternary sediments (Fig. 5H). The ore is generally hosted within mudstones as erratic lenses at two different levels. The lower lens is 2.5 to 3 m thick and occurs in mudstones, whereas the upper lens is separated from the lower by 3 m of mudstone, varying in thickness from 1 to 2 m. These ore lenses trend approximately northeast–southwest and dip northwest between 30° and 50°. The lengths of the first and second ore bodies (from the bottom) vary from 70–80 m to 30–50 m, respectively. Spilitic basalt–ore–mudstone intercalations are overlain by basalt and andesite.

4. Analytical procedures

All samples collected for geochemical analyses were taken representatively from the surface outcrop of ore beds in different locations. Mineralogical results were obtained using conventional optical microscope investigations of 85 polished and thin sections using a Leica DM2500 P. Five ore X-ray diffraction analyses were performed with a Philips PW 3710 diffractometer with a Cu anode operating at a generator voltage of 40 kV and a current of 55 mA; goniometer 2θ values varied from 2° to 70° at a scan rate of 0.04 s/step. Analyses were carried out at the General Directorate of Mineral Research and Exploration laboratories, Ankara, Turkey. The Scanning Electron Microscope (SEM) investigation of four samples was carried out in the Department of Geological Engineering SEM/probe laboratory at Hacettepe University. The SEM was equipped with a Zeiss EVO-50 with a Bruker-Axs XFlash 3001 SDD-EDS, which was operated at less than 15 kV accelerating voltage and 15 nA probe current for element analysis, and 15 kV accelerating voltage and 0.5–1 nA probe current for the images. Fifty-six ore samples were analyzed for major, trace, and REE by ICP-AES, ICP-MS, and NAA methods at the ACME laboratories, Vancouver, Canada. Major oxide, trace element, and REE contents of samples were obtained by ICP-AES using the standard SO-18 values and are given in Tables 1, 2, and 4, respectively.

5. Results and discussion

5.1. Geology

In the study area, the Maden complex hosting the ferromanganese deposits unconformably overlies three different base units, including the Guleman ophiolites, the Pütürge metamorphic rocks, and the Hazar unit. The Guleman ophiolites contain a significant amount of Alpine-type chromite deposits, whereas the Pütürge metamorphic rocks host various industrial raw materials (e.g., pyrophyllite). The

Table 1
Major element analysis (wt %) of 56 ore samples from eight sample localities. (B = Beyhan deposit, P = Palu deposit, S = Sarıkamış deposit, K = Koçkale deposit, G = Germili deposit, H = Hazar deposit, A = Alihan deposit, and KM = Kom deposit).

Sample	SiO_2	Al_2O_3	Fe_2O_3	MgO	CaO	Na_2O	K_2O	TiO_2	P_2O_5	MnO	Cr_2O_3	Mn	Fe	Mn/Fe	Al	Ti
B1	21.34	3.44	38.23	0.81	5.50	0.14	0.10	0.12	1.47	17.78	0.002	13.77	26.76	0.51	1.82	0.07
B2	23.51	3.88	36.95	1.03	5.29	0.05	0.04	0.12	1.35	16.78	0.003	13.00	25.87	0.50	2.05	0.07
B3	29.78	6.92	30.10	4.26	5.44	0.17	0.40	0.17	0.78	16.43	0.003	12.73	21.07	0.60	3.66	0.10
B4	31.65	8.05	26.76	1.23	14.65	0.06	0.04	0.34	0.82	11.20	0.007	8.68	18.73	0.46	4.26	0.20
B5	23.09	4.18	40.97	1.16	3.98	0.04	0.04	0.14	0.26	15.56	0.004	12.05	28.68	0.42	2.21	0.08
B6	36.81	8.00	20.13	1.34	13.18	0.05	0.05	0.31	0.61	11.90	0.003	9.22	14.09	0.65	4.24	0.19
B7	33.01	4.89	24.17	0.88	13.45	0.05	0.02	0.21	0.37	16.63	0.004	12.88	16.92	0.76	2.59	0.13
Average	28.46	5.62	31.04	1.53	8.78	0.08	0.10	0.20	0.81	15.18	0.004	11.76	21.73	0.54	2.98	0.12
P1	34.30	6.47	25.16	1.45	9.14	0.05	0.04	0.20	0.30	15.21	0.002	11.78	17.61	0.67	3.43	0.12
P2	12.26	2.75	39.82	1.01	4.56	0.08	0.04	0.09	0.92	30.26	0.001	23.44	27.87	0.84	1.46	0.05
P3	30.52	5.27	29.56	1.62	6.53	0.04	0.04	0.22	0.43	19.29	0.002	14.94	20.69	0.72	2.79	0.13
P4	25.26	6.70	28.86	1.64	9.57	0.07	0.04	0.23	0.36	20.01	0.002	15.50	20.20	0.77	3.55	0.14
P5	10.55	2.68	42.81	1.19	2.86	0.06	0.06	0.12	1.14	30.25	0.003	23.43	29.97	0.78	1.42	0.07
P6	56.34	1.77	9.03	0.31	1.24	0.10	0.06	0.02	0.17	18.29	0.002	14.17	6.32	2.24	0.94	0.01
P7	10.63	5.52	29.59	0.64	1.51	0.11	0.07	0.32	0.08	39.65	0.001	30.71	20.71	1.48	2.92	0.19
P8	13.97	4.72	42.83	0.93	6.43	0.07	0.06	0.21	0.86	23.70	0.004	18.36	29.98	0.61	2.50	0.13
Average	24.23	4.49	30.96	1.10	5.23	0.07	0.05	0.18	0.53	24.58	0.002	19.04	21.67	0.88	2.38	0.11
S1	22.35	7.86	29.38	2.13	11.87	0.09	0.06	0.31	1.02	15.82	0.005	12.25	20.57	0.60	4.16	0.19
S2	20.02	4.73	34.97	0.76	9.25	0.03	0.03	0.14	0.65	20.69	0.004	16.03	24.48	0.65	2.50	0.08
S3	24.36	4.56	30.30	1.67	12.14	0.03	0.01	0.18	0.61	18.48	0.003	14.32	21.21	0.67	2.41	0.11
S4	25.99	7.19	36.23	3.25	7.31	0.01	0.01	0.41	0.69	14.66	0.005	11.36	25.36	0.45	3.81	0.25
Average	23.18	6.09	32.72	1.95	10.14	0.04	0.03	0.26	0.74	17.41	0.004	13.49	22.90	0.59	3.22	0.16
K1	16.93	5.20	39.90	1.71	12.98	0.06	0.04	0.11	4.06	12.14	0.002	9.40	27.93	0.34	2.75	0.07
K2	19.77	3.58	38.54	1.45	5.50	0.06	0.04	0.14	0.92	19.47	0.001	15.08	26.98	0.56	1.90	0.08
K3	35.33	0.76	0.97	0.16	1.81	0.18	0.04	0.01	0.07	39.42	0.001	30.54	0.68	44.97	0.40	0.01
K4	18.77	4.19	39.29	1.09	9.02	0.15	0.04	0.11	1.67	20.11	0.003	15.58	27.50	0.57	2.22	0.07
K5	19.11	5.08	44.28	1.64	8.30	0.05	0.04	0.14	0.95	13.77	0.003	10.67	31.00	0.34	2.69	0.08
K6	28.13	3.74	31.81	0.52	7.93	0.33	0.04	0.12	0.91	19.44	0.002	15.06	22.27	0.68	1.98	0.07
K7	22.18	4.84	36.71	1.96	8.34	0.24	0.27	0.21	1.42	18.85	0.002	14.60	25.70	0.57	2.56	0.13
K8	18.98	3.41	42.59	1.54	4.55	0.13	0.04	0.16	0.67	17.60	0.001	13.63	29.81	0.46	1.81	0.10
Average	22.40	3.85	34.26	1.26	7.30	0.15	0.07	0.13	1.33	20.10	0.002	15.57	23.98	0.65	2.04	0.08
G1	30.02	4.33	33.71	1.27	5.95	0.07	0.04	0.21	0.61	17.65	0.006	13.67	23.60	0.58	2.29	0.13
G2	27.81	9.00	27.66	1.21	12.28	0.04	0.04	0.36	1.27	14.44	0.004	11.19	19.36	0.58	4.76	0.22
G3	28.82	5.82	31.50	0.83	8.37	0.06	0.04	0.21	0.81	18.14	0.003	14.05	22.05	0.64	3.08	0.13
G4	30.87	4.38	30.59	0.95	7.46	0.09	0.04	0.20	0.71	20.34	0.003	15.76	21.41	0.74	2.32	0.12
Average	29.38	5.88	30.87	1.07	8.52	0.07	0.04	0.25	0.85	17.64	0.004	13.66	21.61	0.63	3.11	0.15
H1	24.77	3.02	35.39	0.76	9.18	0.04	0.04	0.07	1.26	22.30	0.002	17.27	24.77	0.70	1.60	0.04
H2	26.36	2.53	30.66	0.07	16.06	0.09	0.04	0.09	2.13	17.24	0.002	13.35	21.46	0.62	1.34	0.05
H3	20.63	1.92	33.24	0.21	14.70	0.04	0.04	0.07	2.66	23.57	0.007	18.26	23.27	0.78	1.02	0.04
H4	19.76	2.81	40.51	1.26	8.58	0.06	0.04	0.10	1.09	20.83	0.002	16.14	28.36	0.57	1.49	0.06
H5	27.54	5.13	30.09	0.55	13.15	0.05	0.07	0.12	0.73	17.91	0.003	13.87	21.06	0.66	2.72	0.07
H6	27.62	4.14	19.74	0.70	20.35	0.11	0.11	0.14	0.11	20.08	0.003	15.55	13.82	1.13	2.19	0.08
H7	20.21	4.77	36.14	5.02	2.58	0.04	0.04	0.31	0.26	22.13	0.006	17.14	25.30	0.68	2.53	0.19
H8	18.72	1.60	44.21	0.57	8.09	0.08	0.04	0.13	0.37	19.62	0.002	15.20	30.95	0.49	0.85	0.08
H9	23.06	4.47	38.10	0.70	4.88	0.18	0.13	0.12	0.85	18.51	0.017	14.34	26.67	0.54	2.37	0.07
H10	23.14	6.01	34.97	0.62	12.89	0.09	0.04	0.09	1.76	13.77	0.001	10.67	24.48	0.44	3.18	0.05
H11	14.51	4.58	46.98	1.47	3.90	0.08	0.04	0.18	0.40	17.70	0.004	13.71	32.89	0.42	2.42	0.11
H12	9.33	3.80	48.96	1.42	3.06	0.07	0.06	0.24	1.41	20.56	0.002	15.93	34.27	0.46	2.01	0.14
H13	13.78	4.45	54.42	1.86	3.05	0.07	0.17	0.17	0.52	11.15	0.002	8.64	38.09	0.23	2.36	0.10
H14	15.12	4.29	41.40	1.77	5.95	0.06	0.04	0.18	3.66	16.52	0.004	12.80	28.98	0.44	2.27	0.11
Average	20.33	3.82	38.20	1.21	9.03	0.08	0.06	0.14	1.23	18.71	0.004	14.49	26.74	0.54	2.02	0.08
A1	20.81	3.26	41.04	0.33	7.10	0.07	0.02	0.10	2.17	20.08	0.002	15.55	28.73	0.54	1.73	0.06
A2	21.61	3.82	40.12	0.36	6.96	0.01	0.01	0.12	1.05	20.68	0.002	16.02	28.08	0.57	2.02	0.07
A3	22.87	3.91	40.62	0.17	8.44	0.01	0.01	0.11	0.43	18.49	0.002	14.32	28.43	0.50	2.07	0.07
A4	24.49	5.63	30.48	0.56	18.27	0.01	0.02	0.13	0.65	17.96	0.002	13.91	21.34	0.65	2.98	0.08
A5	20.07	2.71	38.38	0.82	14.01	0.01	0.01	0.10	1.39	19.75	0.002	15.30	26.87	0.57	1.43	0.06
A6	21.87	4.47	37.45	1.58	16.24	0.02	0.07	0.16	1.64	13.54	0.002	10.49	26.22	0.40	2.37	0.10
Average	21.95	3.97	38.02	0.64	11.84	0.02	0.02	0.12	1.22	18.42	0.002	14.27	26.61	0.54	2.10	0.07
KM1	22.84	4.37	36.43	0.52	13.82	0.04	0.10	0.11	0.71	16.28	0.002	12.61	25.50	0.49	2.31	0.07
KM2	21.99	3.06	32.28	0.62	12.43	0.04	0.02	0.12	1.13	23.88	0.002	18.50	22.60	0.82	1.62	0.07
KM3	22.38	3.41	40.98	0.52	11.54	0.02	0.03	0.11	0.69	16.25	0.004	12.59	28.69	0.44	1.81	0.07
KM4	25.15	3.67	34.40	0.46	14.04	0.03	0.03	0.09	0.82	18.50	0.002	14.33	24.08	0.60	1.94	0.05
KM5	24.69	4.14	36.81	0.21	13.39	0.04	0.13	0.13	0.74	14.00	0.002	10.85	25.77	0.42	2.19	0.08
Average	23.41	3.73	36.18	0.47	13.04	0.03	0.06	0.11	0.82	17.78	0.002	13.77	25.33	0.54	1.97	0.07

Eocene volcanism in the study area cuts only the Pütürge metamorphic rocks. Geologic, mineralogical, and geochemical studies indicate that these units, including the Guleman ophiolites and the Hazar unit, which are uncomformably overlain by the Maden complex, are not related to ferromanganese mineralization. Although the Eocene volcanic rocks, which cut the Pütürge metamorphic rocks, maybe related to ferromanganese mineralization, we have no evidence that supports this. In a narrow section of the study area, around Germili deposit, the Maden complex is tectonically overlain by the Elazığ magmatic rocks (Fig. 5) and is also tectonically overlain by the Guleman ophiolites outside the southeastern parts of the study area. These thrusts caused greenschist facies metamorphism and affected the entire Maden complex. Ferromanganese mineralization, of course, cannot be affected by this change. However, there are no distinctive

Table 2
Trace element analysis (ppm) of 56 ore samples from eight sample localities. (B = Beyhan deposit, P = Palu deposit, S = Sarıkamış deposit, K = Koçkale deposit, G = Germili deposit, H = Hazar deposit, A = Alihan deposit, and KM = Kom deposit).

Sample	Sc	Ba	Be	Co	Cs	Ga	Hf	Nb	Sr	Th	U	Sb	V	W	Zr	Mo	Cu	Pb	Zn	Ni	As	Co/Zn	Co/Ni
B1	7.0	297.0	2.0	62.3	1.4	6.2	1.1	5.3	429.9	2.0	3.5	2.0	1145.0	10.5	85.3	15.5	857.6	205.0	359.0	828.2	198.3	0.17	0.08
B2	6.0	115.0	3.0	67.3	1.8	8.5	1.0	4.1	172.7	1.6	3.3	1.9	1494.0	10.2	72.3	15.3	87.2	195.5	364.0	856.9	232.2	0.18	0.08
B3	9.0	292.0	2.0	64.4	0.3	9.0	1.2	4.5	1273.6	2.5	1.8	1.5	1329.0	6.5	84.5	8.2	826.6	143.6	312.0	685.7	154.3	0.21	0.09
B4	15.0	523.0	4.0	67.3	0.5	11.5	2.0	6.7	694.1	4.2	2.3	5.9	877.0	13.0	110.3	30.1	252.1	272.8	223.0	539.9	367.4	0.30	0.12
B5	7.0	1712.0	2.0	64.0	0.7	10.6	1.4	6.0	239.2	1.9	3.0	1.3	1800.0	14.7	97.9	19.4	97.9	154.2	247.0	770.8	74.9	0.26	0.08
B6	13.0	1676.0	2.0	87.4	0.4	18.9	2.2	8.5	520.9	5.5	1.5	2.3	802.0	3.7	113.3	56.4	272.4	149.4	234.0	512.6	450.0	0.37	0.17
B7	9.0	462.0	2.0	65.9	0.3	21.6	1.7	6.5	218.1	3.4	2.0	1.0	1472.0	7.2	98.2	43.5	1053.9	136.2	216.0	527.9	99.8	0.31	0.12
Average	9.4	725.3	2.4	68.4	0.8	12.3	1.5	5.9	506.9	3.0	2.5	2.3	1274.1	9.4	94.5	26.9	492.5	179.5	279.3	674.6	225.3	0.24	0.10
P1	9.0	65.0	2.0	64.4	0.6	11.2	1.8	7.1	679.3	2.9	2.8	2.7	613.0	0.4	122.3	16.0	214.2	103.4	238.0	875.3	152.4	0.27	0.07
P2	4.0	450.0	3.0	80.7	0.1	6.8	0.8	2.7	281.3	1.1	2.7	0.8	463.0	9.5	50.8	23.8	495.3	128.2	192.0	457.1	207.0	0.42	0.18
P3	11.0	30.0	1.0	74.2	0.8	10.2	2.0	8.3	538.1	4.3	2.7	3.7	621.0	3.6	122.6	16.9	176.1	105.0	282.0	1004.3	215.4	0.26	0.07
P4	10.0	61.0	2.0	70.9	1.5	10.4	2.0	7.2	713.3	3.4	3.4	2.2	637.0	4.3	117.9	21.4	130.9	122.5	276.0	965.4	214.6	0.26	0.07
P5	6.0	122.0	4.0	96.2	0.2	5.4	0.9	3.5	326.7	1.2	2.6	1.1	337.0	10.1	67.0	20.1	71.8	93.4	228.0	565.4	221.6	0.42	0.17
P6	2.0	41213.0	4.0	32.0	0.6	11.8	0.5	0.9	1303.0	0.7	1.9	1.0	104.0	1.7	15.2	4.2	71.2	32.6	144.0	301.4	49.8	0.22	0.11
P7	9.0	4405.0	12.0	47.8	0.1	10.8	0.6	1.1	469.2	0.7	1.1	0.6	384.0	0.1	23.8	75.8	19.0	43.1	138.0	28.5	18.6	0.35	1.68
P8	10.0	1698.0	3.0	77.8	0.1	10.5	2.2	7.4	1618.7	3.4	3.5	15.2	1292.0	9.8	138.7	13.7	887.7	204.2	347.0	913.4	470.5	0.22	0.09
Average	7.6	6005.5	3.9	68.0	0.5	9.6	1.4	4.8	741.2	2.2	2.6	3.4	556.4	4.9	82.3	24.0	258.3	104.1	230.6	638.9	193.7	0.29	0.11
S1	14.0	50.0	2.0	99.0	0.2	20.9	2.4	8.1	590.1	6.2	1.8	2.1	768.0	7.2	123.8	59.2	915.7	103.9	325.0	828.5	141.5	0.30	0.12
S2	7.0	77.0	2.0	56.6	0.1	23.6	1.1	4.2	333.2	1.9	2.9	3.1	531.0	8.1	77.2	9.1	80.4	103.4	385.0	1028.7	120.8	0.15	0.06
S3	8.0	16.0	2.0	60.6	0.1	21.8	1.5	5.8	117.9	2.8	2.2	1.5	774.0	6.7	96.5	13.7	452.4	126.8	354.0	1153.0	99.3	0.17	0.05
S4	17.0	360.0	2.0	99.1	0.1	18.8	2.2	8.5	2265.0	4.8	1.6	2.5	266.0	5.1	134.1	9.3	669.1	159.0	408.0	899.9	93.9	0.24	0.11
Average	11.5	125.8	2.0	78.8	0.1	21.3	1.8	6.7	826.6	3.9	2.1	2.3	584.8	6.8	107.9	22.8	529.4	123.3	368.0	977.5	113.9	0.21	0.08
K1	6.0	94.0	2.0	62.9	0.1	12.5	0.8	3.4	553.7	1.7	3.3	2.2	1209.0	15.4	64.9	22.3	862.8	140.4	429.0	828.0	426.4	0.15	0.08
K2	7.0	38.0	3.0	69.6	0.2	9.6	1.1	4.0	478.6	1.8	3.9	1.1	1485.0	6.6	74.7	9.4	81.2	186.7	396.0	827.0	178.8	0.18	0.08
K3	1.0	19188.0	4.0	36.7	0.2	5.7	0.5	0.5	1480.2	0.1	1.5	1.0	106.0	0.1	2.9	11.5	38.3	31.6	64.0	75.1	29.8	0.57	0.49
K4	7.0	280.0	2.0	52.8	0.1	10.0	0.8	3.4	314.8	1.4	3.0	1.6	668.0	7.7	63.8	10.6	289.6	146.2	398.0	679.0	227.5	0.13	0.08
K5	7.0	120.0	3.0	60.0	0.1	12.8	1.0	3.5	387.0	1.4	4.5	1.4	886.0	4.7	72.5	8.7	885.0	152.3	423.0	719.3	173.1	0.14	0.08
K6	6.0	460.0	1.0	55.4	0.7	11.6	1.0	3.7	425.9	1.5	3.1	1.6	1280.0	10.9	72.9	18.5	773.5	138.6	262.0	711.3	192.9	0.21	0.08
K7	10.0	1155.0	3.0	73.0	0.2	7.9	1.7	6.7	3208.0	3.3	2.7	1.6	518.0	7.7	120.2	7.2	971.5	293.0	373.0	759.8	225.9	0.20	0.10
K8	7.0	42.0	2.0	74.0	0.2	9.1	1.0	4.0	408.4	2.4	3.5	1.6	1593.0	6.2	76.6	8.1	92.0	190.2	401.0	889.7	155.9	0.18	0.08
Average	6.4	2672.1	2.5	60.6	0.2	9.9	1.0	3.7	907.1	1.7	3.2	1.5	968.1	7.4	68.6	12.0	499.2	159.9	343.3	686.2	201.3	0.18	0.09
G1	12.0	123.0	1.0	61.0	0.1	7.4	1.7	7.1	6892.6	3.4	1.3	2.2	226.0	2.4	128.6	3.8	110.9	71.2	293.0	1055.6	255.4	0.21	0.06
G2	16.0	226.0	2.0	84.8	0.1	11.0	2.4	9.8	9537.7	5.3	2.5	2.0	257.0	4.4	138.8	3.7	41.9	134.2	214.0	678.4	335.7	0.40	0.13
G3	11.0	100.0	3.0	77.1	0.1	8.7	1.8	7.4	5761.2	3.0	2.9	1.8	393.0	3.1	108.4	3.2	97.9	103.1	206.0	866.8	290.8	0.37	0.09
G4	10.0	74.0	3.0	59.4	0.1	7.8	1.6	7.1	5735.3	3.0	2.6	1.8	351.0	2.7	105.5	2.9	63.0	74.5	172.0	726.6	265.4	0.35	0.08
Average	12.3	130.8	2.3	70.6	0.1	8.7	1.9	7.9	6981.7	3.7	2.3	2.0	306.8	3.2	120.3	3.4	78.4	95.8	221.3	831.9	286.8	0.32	0.08
H1	4.0	129.0	1.0	65.4	0.1	8.3	0.7	2.5	243.7	1.1	3.5	2.1	673.0	3.3	57.1	7.6	51.7	117.1	240.0	841.4	169.1	0.27	0.08
H2	5.0	75.0	2.0	60.3	0.1	8.7	0.7	3.0	176.2	1.2	3.2	1.4	553.0	8.3	61.8	9.3	73.4	84.4	293.0	574.9	197.6	0.21	0.10
H3	4.0	273.0	1.0	76.1	0.1	12.2	0.5	2.3	211.6	1.0	4.4	2.5	1107.0	5.9	51.9	16.0	16.2	77.7	379.0	1207.6	168.6	0.20	0.06
H4	5.0	38.0	3.0	52.3	0.2	9.2	0.7	3.7	189.9	1.4	3.2	1.3	446.0	4.5	62.0	6.1	221.0	126.4	296.0	548.0	151.2	0.18	0.10
H5	5.0	58.0	2.0	51.7	0.4	11.0	0.9	3.9	294.7	1.3	2.6	1.2	365.0	3.8	75.5	5.5	52.5	160.5	91.0	723.1	176.3	0.57	0.07
H6	5.0	26.0	2.0	42.0	0.2	8.0	0.7	1.8	736.2	1.4	0.7	0.5	563.0	0.1	48.6	4.7	5448.3	55.3	186.0	566.4	96.2	0.23	0.07
H7	12.0	52.0	1.0	95.0	0.1	8.2	1.1	3.3	236.6	1.1	2.1	0.8	376.0	2.2	81.4	4.6	388.3	195.3	723.0	983.9	176.8	0.13	0.10
H8	7.0	40.0	2.0	76.7	0.1	5.8	1.3	4.3	700.7	1.3	3.2	1.8	245.0	2.3	86.5	4.4	198.5	131.6	345.0	741.4	96.7	0.22	0.10
H9	6.0	1182.0	2.0	57.4	3.1	7.5	1.4	3.9	1070.1	2.1	2.5	1.6	396.0	3.0	80.0	5.4	180.1	71.1	355.0	753.4	147.9	0.16	0.08
H10	4.0	64.0	3.0	54.8	0.1	12.3	0.7	2.9	636.0	1.4	3.3	1.5	1512.0	7.4	63.7	13.0	289.3	215.7	346.0	445.6	343.1	0.16	0.12
H11	9.0	933.0	4.0	71.4	1.0	20.0	2.2	8.9	553.2	4.0	2.9	1.7	534.0	5.1	139.5	5.0	177.9	253.0	408.0	606.0	143.7	0.18	0.12
H12	10.0	256.0	2.0	72.5	0.7	22.0	1.3	8.5	1104.0	2.7	1.8	1.5	520.0	8.9	86.0	7.9	1136.1	209.6	457.0	882.9	234.0	0.16	0.08
H13	9.0	282.0	2.0	67.8	1.1	18.2	1.5	5.5	835.6	3.1	2.1	1.6	429.0	7.4	104.2	4.3	124.8	206.2	442.0	606.9	133.9	0.15	0.11
H14	8.0	5407.0	2.0	76.7	1.4	21.7	1.7	6.5	465.9	3.0	3.1	2.4	576.0	5.9	102.8	6.5	144.6	190.6	448.0	577.8	714.3	0.17	0.13
Average	6.6	629.6	2.1	65.7	0.6	12.4	1.1	4.4	532.5	1.9	2.8	1.6	592.5	4.9	78.6	7.2	607.3	149.6	357.8	718.5	210.7	0.18	0.09
A1	6.0	2598.0	2.0	73.9	0.5	18.5	1.2	5.9	655.5	1.9	2.4	2.8	366.0	4.9	80.9	6.2	503.9	135.8	338.2	941.7	282.3	0.22	0.08
A2	6.0	3888.0	2.0	72.0	0.5	21.1	1.0	4.5	317.8	1.7	2.5	2.3	693.0	3.3	90.4	5.4	500.1	260.5	356.6	935.9	206.5	0.20	0.08
A3	6.0	826.0	2.0	69.4	0.9	21.1	1.2	5.3	253.2	1.8	2.9	1.1	503.0	3.6	103.3	5.2	230.8	127.9	290.2	715.1	139.2	0.24	0.10
A4	5.0	1509.0	2.0	65.9	0.1	27.8	1.0	5.2	296.5	1.3	0.9	1.3	1072.0	3.0	66.8	10.2	1236.4	75.4	190.3	836.7	156.6	0.35	0.08
A5	5.0	505.0	2.0	63.8	0.1	22.5	1.0	4.5	305.6	1.7	4.9	2.2	1325.0	5.2	62.8	8.1	956.8	145.7	275.4	853.2	178.6	0.23	0.07
A6	8.0	174.0	3.0	57.4	0.4	16.5	1.6	5.3	2096.9	2.8	1.7	2.2	356.0	2.9	212.4	6.1	843.5	90.4	230.9	705.7	140.4	0.25	0.08
Average	6.0	1583.3	2.2	67.1	0.4	21.3	1.2	5.1	654.3	1.9	2.6	2.0	719.2	3.8	102.8	6.9	711.9	139.3	280.3	831.4	183.9	0.24	0.08
KM1	6.0	17.0	3.0	54.1	0.6	14.8	1.3	3.1	174.8	1.9	2.0	0.9	498.0	3.7	71.0	4.8	43.7	102.2	164.0	492.3	153.7	0.33	0.11
KM2	6.0	661.0	2.0	62.0	0.3	20.8	0.9	3.7	131.6	1.3	2.6	1.4	698.0	4.7	63.6	7.3	28.1	138.1	285.0	845.5	353.6	0.22	0.07
KM3	6.0	20.0	2.0	38.7	0.5	16.8	1.0	3.1	48.3	1.8	2.0	1.4	247.0	3.5	63.6	7.5	342.4	236.1	106.0	460.5	223.2	0.37	0.08
KM4	4.0	65.0	2.0	53.2	0.3	22.4	1.1	3.3	49.1	1.2	1.7	0.8	727.0	2.3	62.8	5.3	991.7	89.9	231.0	455.7	227.4	0.23	0.12
KM5	6.0	15.0	1.0	58.9	0.7	22.9	0.7	3.3	201.2	1.6	1.5	1.0	797.0	4.8	63.3	3.9	74.2	90.4	172.0	362.6	138.4	0.34	0.16
Average	5.6	155.6	2.0	53.4	0.5	19.5	1.0	3.3	121.0	1.6	2.0	1.1	593.4	3.8	64.9	5.8	296.0	131.3	191.6	523.3	219.3	0.28	0.10

geologic, mineralogical, and geochemical differences between the Germili deposit, in which the only tectonic overlay is by the Elazığ magmatic rocks, and other ferromanganese deposits in the study area. We conclude that the influence of the thrusts affected all areas. The Koçkale ferromanganese deposit has the highest of the ore beds when compared to the other studied deposits (Fig. 5), in which spilitic basalts and diabase dykes, which belong to the volcano-sedimentary Melafan formation of the Maden complex, are also thick. There is a linear relationship between the thickness of volcanic rocks that belong to the Melafan formation and the thickness of ferromanganese ore. In addition, in the Germili deposit, the thickness of mudstones is small as much as a few centimeters. There are mudstone intercalations in the ferromanganese mineralization that directly lie on the spilitic basalt and diabase. Stratigraphically, mudstone intercalations gradually increase to the higher levels of the unit. Sulfide ores exist within the matrix of basal conglomerates in the Ceffan formation of the Maden complex. The presence of tuffite in the Arbo formation that lies on the Ceffan formation suggests early volcanism. Spilitic basalt and diabase, with variable thickness, are commonly found in the lower parts of the Melafan formation. The thickness of these volcanic rocks gradually decreases toward the upper levels of the formation. Volcanic rocks in the lower parts of the formation contain sulfide mineralization in almost every area. This volcanism is probably responsible for the formation of ferromanganese deposits in the Malatya and Elazığ regions. In the Elazığ–Malatya region, the Mn–Fe mineralizations are mainly located within the lower levels of the mudstones, and some lie directly on the spilitic basalts of the volcano-sedimentary part of the Maden complex (Figs. 3–5). At the base of the Beyhan, Germili, Hazar, and Alihan deposits, the Mn–Fe mineralizations occur as lenses that lie directly above the spilitic basalts. Toward the upper section, the ferromanganese mineralization is within interbedded with mudstones. At the Palu, Sarıkamış, Koçkale, and Kom deposits, the Mn–Fe mineralizations occur as lenses within the mudstones. Recent field studies at these eight localities suggest that the manganese deposits from the Elazığ–Malatya region are associated with the mudstone member of the Maden complex. The Mn–Fe mineralization as lenses and interbedded layers within the mudstones in the Elazığ–Malatya region suggests that both ferromanganese ores and mudstones are of the same age. Underlying spilitic basalts and diabases show veining of copper oxides throughout the Elazığ–Malatya region suggesting evidence of hydrothermal activity. The presence of massive sulfide deposits, including Malatya–Pütürge–Çanakçı copper (Emin, 1979), Elazığ–Maden copper (Erler, 1983), and 22 small occurrences within the Maden complex (Fig. 3), indicates that at one time a powerful hydrothermal system was active. Although all the Mn–Fe occurrences within the Maden complex are at a stratigraphically higher level than the massive sulfide deposits, the Mn–Fe and sulfide deposits may be cogenetic with the sulfide deposits forming at depth, and the Mn–Fe precipitated at or near the sea floor.

5.2. Mineralogy of the Mn–Fe deposits

Manganese oxides are deposited in a variety of terrestrial and marine environments as a result of supergene and hydrothermal processes (Nicholson, 1992a; Roy, 1992). Manganese minerals, like pyrolusite and psilomelane, are known to occur in a variety of environments (supergene marine, weathered, and hydrothermal deposits) (Nicholson, 1992a). Manganese minerals, such as braunite, bixbyite, and jacobsite, are known to occur in hydrothermal deposits (Hewett and Fleischer, 1960; Nicholson, 1992a).

Manganese minerals in decreasing amounts in the Elazığ–Malatya Mn–Fe deposits are braunite, bixbyite, jacobsite, pyrolusite, manganite, and psilomelane. Braunite is the most abundant manganese mineral in Mn–Fe deposits of the Middle Eocene Maden complex, which was metamorphosed to lower greenschist facies conditions (Bozkaya et al., 2006). According to Maynard (2003, 2010) Eocene and younger Mn–Fe deposits have a mineral, usually an oxide, other than braunite; braunite might be the result of amorphous silica in the host rocks. The origin of the braunite in the Mn–Fe deposits of

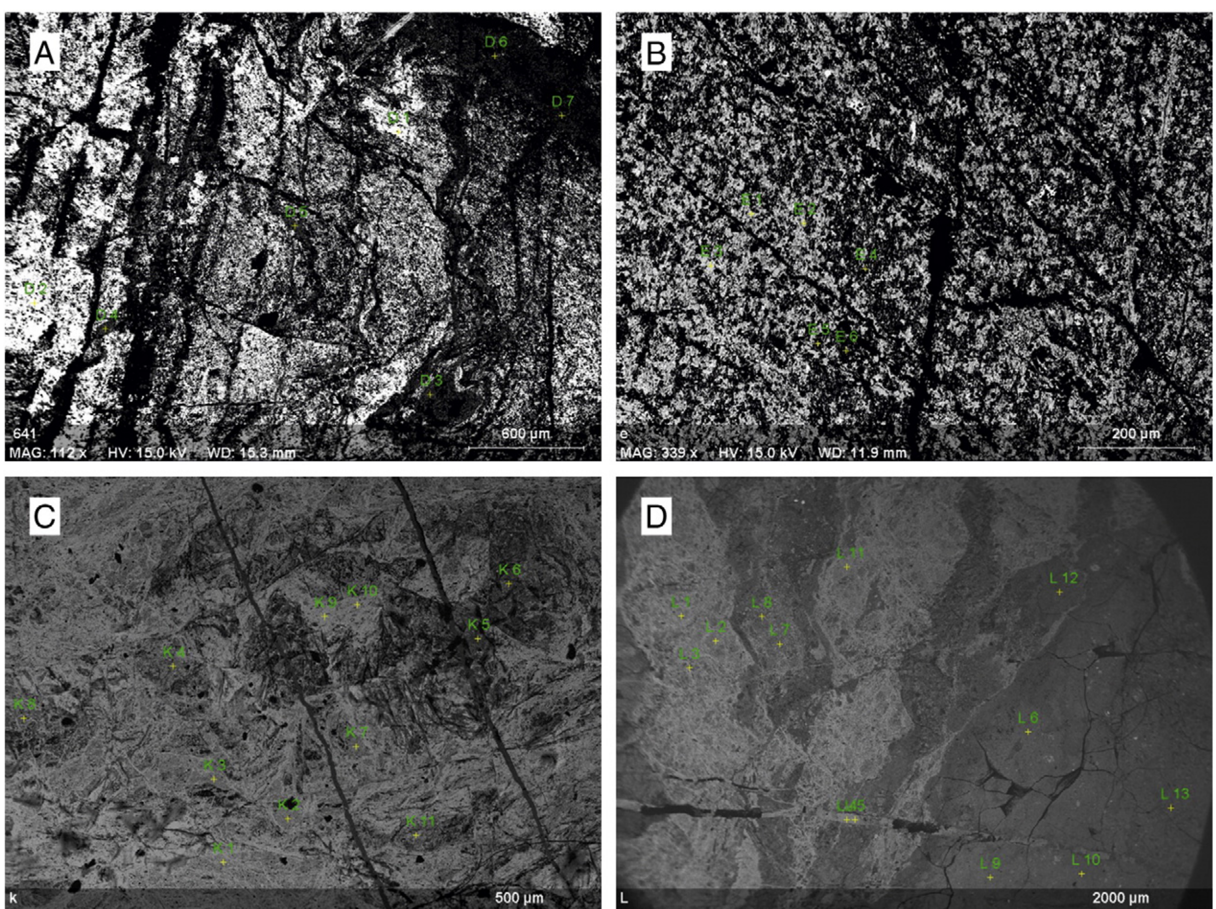

Fig. 6. Back-scattered electron SEM images from ferromanganese ore deposits. (A) Germili deposit (D1, D2 = bixbyite; D3 to D7 = clay minerals rich in iron and manganese). (B) Koçkale deposit (E1 = hematite; E2, E4, E5 = braunite; E3 = pyrolusite; E6 = clay minerals rich in iron and manganese). (C) Hazar deposit (K1, K2, K3 = psilomelane; K4, K7, K8, K11 = braunite; K5, K6, K9, K10 = bixbyite). (D) Beyhan deposit (L1, L2, L3, L11 = bixbyite; L4, L5 = pyrolusite; L6, L7,L8, L9, L10, L12, L13 = braunite).

Table 3
Major and trace element contents of various types of manganese deposits. Analyses taken from (1) = Shah and Moon (2007), (2, 3, 4, 5) = Choi and Hariya (1992), (6) = Gültekin (1998), (7) = Oygür (1990), and (8) = Koç et al. (2000).

Countries	Pakistan (1)	Japan (2)	Japan (3)	Japan (4)	Japan (5)	Turkey (6)	Turkey (7)	Turkey (8)	This study							
Regions	Hazara	Wakasa	Koryu	Hinode	Tokora	Binkılıç	Çayırlı	Kasımağa	Beyhan	Palu	Sarıkamış	Koçkale	Germili	Hazar	Alihan	Kom
Origins	Hydrothermal–hydrogenous	Hydrothermal	Hydrothermal	Sedimentary	Sedimentary	Sedimentary	Volcano-sedimentary	Volcano-sedimentary								
SiO_2 (%)	9.41	58.16	40.56	12.67	32.04	10.65	63.02	13.43	28.46	24.23	23.18	22.40	29.38	20.33	21.95	23.41
TiO_2 (%)	0.84	0.04	0.05	0.04	0.91	0.02	0.03	0.1	0.20	0.18	0.26	0.13	0.25	0.14	0.12	0.11
Al_2O_3 (%)	12.53	0.55	0.63	1.27	8.82	2.85	0.65	2.95	5.62	4.49	6.09	3.85	5.88	3.82	3.97	3.73
Fe_2O_3 (%)	20.33	0.92	0.55	0.59	38.32	2.46	0.68	14.33	31.34	30.96	32.72	34.26	30.87	38.20	38.02	36.18
MnO (%)	33.78	32.5	42.06	67.21	5.22	33.39	29.22	40.43	15.18	24.58	17.21	20.10	17.64	18.71	18.42	17.78
MgO (%)	0.59	0.19	0.02	0.08	4.04	1.27	0.2	12.72	1.53	1.10	1.95	1.26	1.07	1.21	0.64	0.47
CaO (%)	6.43	4.15	1.65	1.67	8.82	18.96	0.24	6.82	8.78	5.23	10.14	7.30	8.52	9.03	11.84	13.04
Na_2O (%)	0.07	0.04	0.11	0.07	0.82	0.39	0.05	0.06	0.08	0.07	0.04	0.15	0.07	0.08	0.02	0.03
K_2O (%)	0.88	0.1	0.27	0.46	0.26	0.56	0.11	0.19	0.10	0.05	0.03	0.07	0.04	0.06	0.02	0.06
P_2O_5 (%)	3.73	0.1	0.02	0.12	0.62	0.31	0.04	0.08	0.81	0.53	0.74	1.33	0.85	1.23	1.22	0.82
Ba (ppm)	6304	13.79	22126	8.06	99	6892	1229.4	2719.4	725.29	6005.50	125.75	2672.13	130.75	629.64	1583.33	155.60
V (ppm)	573	258	211	468	1637	106	143.7	106.1	1274.14	556.38	584.75	968.13	306.75	592.50	719.20	593.40
Cr	247	10	7	16	186	26	13.7	10	27.00	14.00	27.00	14.00	27.00	27.00	14.00	14.00
Co	404	2	118	222	433	59	25.21	49.5	68.37	68.00	78.83	60.55	70.58	65.72	67.07	53.38
Ni	305	28	351	341	432	167	69.4	23	674.57	638.85	977.53	686.15	831.85	718.52	831.40	523.32
Cu	375	50	1174	691	500	26	154.9	126.8	492.53	258.28	529.40	499.24	78.43	607.34	711.90	296.02
Zn	580	26	129	147	374	49	66.7	63.5	279.29	230.63	368.00	343.25	221.25	357.79	280.30	191.60
Pb	2357	112	14	18	267	–	6.5	53.5	179.53	104.05	123.28	159.88	95.75	149.61	128,00	131.34
Th	31	2	2	98	4	–	0.4	433.2	3.01	2.21	3.93	1.70	3.68	1.86	1.87	1.56
Rb	24	2	3	4	5	–	2.9	5	2.67	0.76	0.45	1.54	0.55	1.42	0.75	0.82
Sr	–	85	483	260	102	2100	243.4	255	506.9	741.2	826.6	907.1	6981.7	532.5	655.90	121.0
Y	–	5	–	–	80	15	33	22.2	125.90	114.95	138.00	138.09	163.95	132.41	122.50	114.30
Nb	–	3	8	4	4	–	0.7	11.1	5.94	4.78	6.65	3.65	7.85	4.36	5.10	3.30
Zr	–	12	62	48	104	32	4	26.9	94.54	82.29	107.90	68.56	120.33	78.64	102.80	64.86
As	–	–	–	–	–	–	–	213	225.27	193.74	113.88	201.29	286.83	210.67	183.90	219.26

the Elazığ–Malatya region may be related to late diagenetic and/or early metamorphic processes, but there is insufficient evidence for these changes and for the later introduction of the silica. The most probable source of silica is submarine volcanism.

Identified minerals in the Germili, Koçkale, Hazar, and Beyhan deposit are shown in Fig. 6A to D. Some Mn oxide minerals were observed in the fractures as late-stage fracture fillings. Bixbyite and braunite are the main ore minerals.

5.3. Major and trace elements in the manganese oxides

Analytical results of the major and trace elements of the Maden complex Mn–Fe deposits are given in Tables 1 and 2. Major and trace element contents of different types of manganese deposits are shown in Table 3 for comparison. Based on the analysis of randomly collected 56 ore samples from the eight deposits, indicate that the Mn–Fe ore are relatively homogeneous with most samples having an Mn:Fe ratio less than 1. Manganese ranges from 8.64 to 30.71 wt.% (average = 14.74), and Fe ranges from 0.68 to 38.09 wt.% (average = 24.22) in the Maden complex Mn–Fe deposits. Mn:Fe ratios of the deposits are 0.23–2.24 (average = 0.63) (except K3, which is pure manganese ore). The Mn:Fe ratios of 52 samples range from 0.1 to 1; three samples have a ratio between 1 and 3, and one sample has a high ratio (see Table 1). These values are comparable with those of SEDEX (i.e., sedimentary-exhalative) deposits (0.1 < Mn:Fe < 10), as defined by Nicholson et al. (1997).

The hydrogenous and hydrothermal deposits can be distinguished by using Co:Ni and Co:Zn ratios (Toth, 1980). A ratio of Co:Ni < 1 and Co:Ni > 1 indicates a sedimentary origin and a deep marine environment, respectively (Delian, 1994; Fernandez and Moro, 1998; Öksüz, 2011). Co:Ni ratios in the Maden complex Mn–Fe deposits range from 0.05 to 1.68 (average = 0.09). Co:Ni ratios are lower than 1 in 55 samples and higher than 1 in one sample (i.e., sample P7 in the Palu deposit; see Table 2). Co:Zn ratios of 0.15 indicate hydrothermal-type deposits, while Co:Zn ratios of 2.5 indicate hydrogenous-type deposits (Toth, 1980). Co:Zn ratios in the Maden complex Mn–Fe deposits range from 0.13 to 0.57 (average = 0.23). Co:Zn ratios are around 0.15 (i.e., ≤0.15) in six samples and greater than 0.15 in 50 samples (see Table 2). Although Co:Zn ratios from the Maden complex Mn–Fe deposits point to a hydrothermal source for Mn–Fe mineralization, Co:Ni ratios of ore samples indicate that sedimentary environments played an important role during the formation of the Mn–Fe deposits.

Trace element content of As, Ba, Cu, Li, Mo, Pb, Sb, Sr, V, and Zn shows an enrichment tendency in oxide ores deposited from hydrothermal fluids (Nicholson, 1992a and references therein). All the studied ferromanganese ores display an enrichment trend of As, Ba, Cu, Mo, Pb, Sr, V, and Zn that is similar to deposits formed from hydrothermal fluids (see Table 2). The amount of Zn is generally expected to be fractionated in hydrothermal systems through concentration in proximal sulfide deposits (Hein et al., 2008). Zinc concentrations in these ferromanganese ores range from 64 to 723 ppm (average = 296), these relatively high Zn content of ores are probably indicative of the leaching processes from sulfide mineralization at greater depths. High Ni as well as Cr contents probably reflect the incorporation of a detrital ultramafic component or the leaching of ultramafic rocks; Ni also occurs in sulfides and therefore has multiple sources. If high Ni is not accompanied by high Cr, then an ultramafic component may not be indicated (Hein et al., 2008). Nickel concentrations in the studied ores range from 28.5 to 1207.6 ppm (average = 718), while Cr concentrations range from 7 to 116 ppm (average = 21). Compared

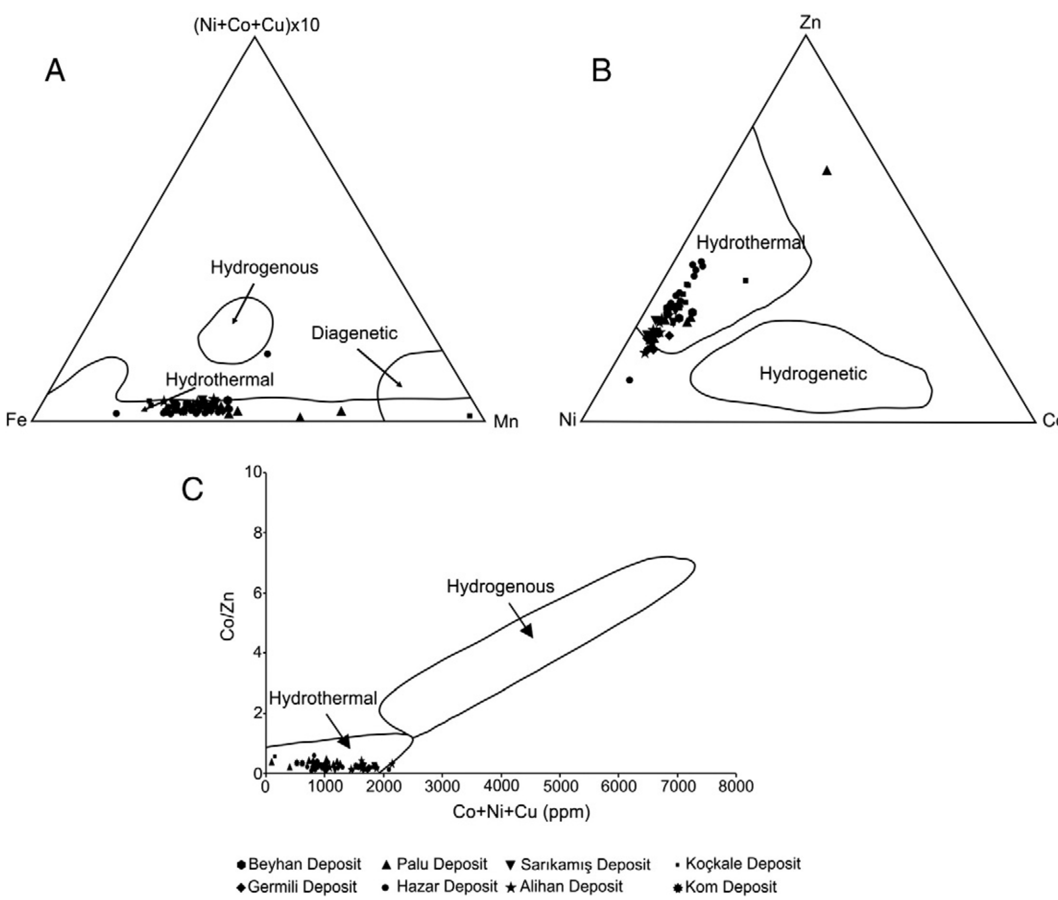

Fig. 7. Discrimination diagrams for manganese deposits. (A) Mn–Fe–(Ni + Co + Cu)x10 discrimination diagram (Bonatti et al., 1972; Crerar et al., 1982), (B) Zn–Ni–Co discrimination diagram (Choi and Hariya, 1992) and (C) Co/Zn–Co + Ni + Cu discrimination diagram (Toth, 1980).

Table 4
REE concentrations (ppm) of 56 ore samples from eight localities. (B = Beyhan deposit, P = Palu deposit, S = Sarıkamış deposit, K = Koçkale deposit, G = Germili deposit, H = Hazar deposit, A = Alihan deposit, and KM = Kom deposit).

Sample	La	Ce	Pr	Nd	Sm	Eu	Gd	Tb	Dy	Ho	Er	Tm	Yb	Lu	Y	ΣREE	LREE/HREE	La/Ce	La_N/Nd_N	Dy_N/Yb_N	Ce/Ce*	Eu/Eu*
B1	148.60	39.60	35.81	150.70	26.90	6.69	29.62	4.96	25.33	4.55	13.66	1.69	10.85	1.55	129.10	500.51	4.43	3.75	1.91	1.52	0.13	0.72
B2	149.80	36.50	35.67	148.00	27.10	6.66	28.96	4.86	24.60	4.47	13.34	1.63	10.93	1.51	135.40	494.03	4.47	4.10	1.96	1.46	0.12	0.72
B3	150.80	48.70	35.25	140.70	25.20	6.49	28.64	4.80	25.22	4.52	13.85	1.74	11.02	1.59	134.50	498.52	4.46	3.10	2.07	1.49	0.16	0.74
B4	147.90	74.70	37.07	152.20	27.80	6.76	29.91	5.04	24.94	4.59	13.48	1.69	11.13	1.63	132.30	538.84	4.83	1.98	1.88	1.45	0.24	0.71
B5	145.40	43.90	34.38	136.80	25.60	6.08	26.51	4.52	22.94	4.04	12.45	1.59	10.31	1.42	105.70	475.94	4.68	3.31	2.06	1.44	0.15	0.71
B6	138.80	89.70	36.84	154.10	28.40	6.65	29.47	4.94	24.94	4.32	12.92	1.57	10.86	1.55	126.90	545.06	5.02	1.55	1.74	1.49	0.30	0.70
B7	160.00	60.40	36.50	144.00	27.50	7.02	28.75	4.43	22.91	4.70	12.94	1.87	10.65	1.56	117.40	523.23	4.96	2.65	2.15	1.40	0.19	0.76
Average	148.76	56.21	35.93	146.64	26.93	6.62	28.84	4.79	24.41	4.46	13.23	1.68	10.82	1.54	125.90	510.88	4.69	2.65	1.96	1.46	0.19	0.72
P1	167.70	71.00	44.34	182.70	33.00	7.65	33.23	5.52	28.40	4.82	14.06	1.71	11.31	1.54	114.60	606.98	5.03	2.36	1.78	1.63	0.20	0.70
P2	109.10	23.50	24.59	103.60	18.40	4.63	20.52	3.37	18.67	3.15	9.65	1.18	7.83	1.15	96.80	349.34	4.33	4.64	2.04	1.55	0.11	0.73
P3	176.00	79.30	45.61	185.50	34.20	8.26	35.70	6.07	30.86	5.38	15.58	1.91	12.88	1.80	138.80	639.05	4.80	2.22	1.84	1.56	0.21	0.72
P4	188.30	72.50	46.96	194.80	34.80	8.28	35.57	6.06	30.45	5.56	16.58	2.05	13.51	1.85	146.30	657.27	4.89	2.60	1.87	1.46	0.19	0.71
P5	141.10	33.30	32.01	135.60	23.80	6.17	27.81	4.50	23.84	4.35	13.10	1.56	10.10	1.42	128.00	458.66	4.29	4.24	2.01	1.53	0.12	0.73
P6	43.00	12.50	10.61	45.10	7.90	1.68	9.10	1.63	9.29	1.70	5.82	0.77	4.81	0.74	51.20	154.65	3.57	3.44	1.85	1.25	0.14	0.60
P7	22.00	26.70	3.60	16.80	3.70	1.22	5.56	0.91	5.14	0.93	3.00	0.32	2.19	0.33	35.90	92.40	4.03	0.82	2.53	1.52	0.72	0.82
P8	229.60	55.50	51.54	218.90	37.40	9.44	41.31	7.15	37.77	6.94	20.63	2.49	17.21	2.35	208.00	738.23	4.43	4.14	2.03	1.42	0.12	0.73
Average	134.60	46.79	32.41	135.38	24.15	5.92	26.10	4.40	23.05	4.10	12.30	1.50	9.98	1.40	114.95	462.07	4.58	2.88	1.92	1.50	0.17	0.72
S1	188.20	91.60	42.50	174.40	33.07	8.21	36.68	5.44	28.95	6.10	16.17	2.25	13.27	1.94	155.10	648.78	4.86	2.05	2.09	1.42	0.25	0.72
S2	165.80	35.20	34.42	139.40	25.84	6.69	29.54	4.47	24.54	5.18	14.44	1.93	11.10	1.64	132.50	500.19	4.39	4.71	2.30	1.43	0.11	0.74
S3	165.60	51.80	37.84	154.90	28.72	7.06	30.70	4.63	24.32	4.99	13.56	1.88	11.24	1.62	116.40	538.86	4.80	3.20	2.07	1.40	0.16	0.72
S4	201.50	88.50	45.39	182.20	35.17	8.86	38.36	5.78	31.06	6.42	17.26	2.38	14.14	2.08	148.00	679.10	4.78	2.28	2.14	1.43	0.22	0.73
Average	180.28	66.78	40.04	162.73	30.70	7.71	33.82	5.08	27.22	5.67	15.36	2.11	12.44	1.82	138.00	591.73	4.72	2.70	2.14	1.42	0.19	0.73
K1	169.70	31.30	37.06	151.70	26.90	7.13	31.84	5.24	27.44	5.05	14.71	1.92	12.26	1.73	163.20	523.98	4.23	5.42	2.17	1.45	0.09	0.74
K2	171.80	41.50	40.86	167.00	30.20	7.65	32.88	5.50	28.81	5.08	15.20	1.83	12.28	1.67	150.20	562.26	4.45	4.14	1.99	1.52	0.12	0.74
K3	19.00	5.70	3.96	15.80	3.20	0.64	4.02	0.76	4.53	0.86	2.74	0.38	2.45	0.35	20.00	64.39	3.00	3.33	2.33	1.20	0.16	0.55
K4	163.40	27.70	37.93	163.60	28.00	7.39	34.26	5.61	29.80	5.64	16.84	2.03	13.29	1.79	182.90	537.28	3.92	5.90	1.93	1.46	0.08	0.73
K5	145.10	30.70	32.73	138.90	25.10	6.43	28.30	4.76	24.81	4.65	13.81	1.68	11.01	1.55	144.90	469.53	4.18	4.73	2.02	1.46	0.11	0.74
K6	150.30	40.10	35.78	147.50	26.30	6.53	28.62	4.83	25.43	4.35	12.92	1.64	10.81	1.47	127.20	496.58	4.51	3.75	1.97	1.53	0.13	0.72
K7	210.60	69.50	47.70	201.20	34.80	8.50	38.70	6.53	33.80	6.20	18.56	2.24	15.31	2.14	183.40	695.78	4.63	3.03	2.03	1.43	0.17	0.71
K8	153.00	38.90	35.54	147.90	26.60	6.77	29.15	4.98	26.15	4.59	13.92	1.66	11.11	1.53	132.90	501.80	4.39	3.93	2.00	1.53	0.13	0.74
Average	147.86	35.68	33.95	141.70	25.14	6.38	28.47	4.78	25.10	4.55	13.59	1.67	11.07	1.53	138.09	481.45	4.31	4.14	2.02	1.47	0.12	0.73
G1	184.80	70.00	47.09	193.60	35.80	8.71	37.20	6.36	32.30	5.60	16.58	2.05	13.84	1.87	158.90	655.80	4.66	2.64	1.85	1.51	0.18	0.72
G2	193.00	111.70	47.59	196.40	34.80	8.44	37.58	6.31	31.90	5.88	17.84	2.22	14.70	2.03	176.20	710.39	5.00	1.73	1.90	1.41	0.28	0.71
G3	203.10	70.90	49.18	200.50	36.90	8.88	39.78	6.72	33.77	6.14	17.70	2.22	14.31	1.99	170.80	692.09	4.64	2.86	1.96	1.53	0.17	0.70
G4	187.60	66.50	47.15	193.00	34.30	8.42	36.95	6.15	31.87	5.55	16.65	2.07	13.48	1.90	149.90	651.59	4.68	2.82	1.88	1.53	0.17	0.72
Average	192.13	79.78	47.75	195.88	35.45	8.61	37.88	6.39	32.46	5.79	17.19	2.14	14.08	1.95	163.95	677.47	4.75	2.41	1.90	1.50	0.20	0.71
H1	145.60	25.40	32.78	136.50	24.20	6.04	27.29	4.62	25.22	4.73	14.55	1.73	11.17	1.58	156.50	461.41	4.08	5.73	2.06	1.47	0.09	0.72
H2	162.90	31.40	39.28	165.00	29.10	7.20	31.11	5.24	26.86	4.77	14.40	1.76	11.42	1.57	144.80	532.01	4.48	5.19	1.91	1.53	0.09	0.73
H3	134.30	21.50	24.18	103.30	17.50	4.40	22.01	3.58	20.29	3.82	12.44	1.50	9.74	1.36	140.40	379.92	4.08	6.25	2.52	1.35	0.09	0.69
H4	128.00	28.90	26.82	117.00	20.60	5.34	24.91	4.15	23.21	4.06	12.66	1.54	10.14	1.41	132.90	408.74	3.98	4.43	2.12	1.49	0.12	0.72
H5	151.20	36.60	35.73	146.70	26.10	6.20	26.85	4.51	22.65	3.95	11.96	1.46	9.55	1.35	113.40	484.81	4.89	4.13	1.99	1.54	0.12	0.71
H6	92.90	23.10	22.36	90.60	16.50	3.97	17.90	2.98	15.78	2.69	8.27	0.99	6.72	0.95	67.20	305.71	4.43	4.02	1.98	1.52	0.12	0.70
H7	176.90	31.50	36.39	150.60	26.20	6.59	29.68	5.10	27.05	4.85	14.66	1.76	11.98	1.65	134.70	524.91	4.43	5.62	2.27	1.47	0.09	0.72
H8	140.60	35.80	33.75	144.20	25.70	6.36	28.28	4.78	25.01	4.43	13.51	1.58	10.84	1.46	122.20	476.30	4.30	3.93	1.89	1.50	0.13	0.72
H9	127.10	29.90	27.60	118.20	20.80	5.33	23.60	3.98	21.66	3.81	11.88	1.44	9.41	1.32	114.20	406.03	4.27	4.25	2.08	1.49	0.12	0.73
H10	142.50	30.80	31.85	137.50	24.40	6.10	27.51	4.57	24.93	4.31	13.23	1.61	10.56	1.49	149.90	461.36	4.23	4.63	2.01	1.53	0.11	0.72
H11	158.50	57.20	35.34	146.40	28.38	7.60	32.19	4.98	26.63	5.22	14.57	2.03	11.74	1.68	131.40	532.46	4.38	2.77	2.10	1.47	0.18	0.77
H12	173.10	41.90	33.80	139.90	25.25	6.72	28.72	4.35	23.95	4.92	13.76	1.89	11.12	1.61	132.40	510.99	4.66	4.13	2.39	1.40	0.13	0.76
H13	184.20	49.80	39.52	157.80	30.63	8.09	34.19	5.15	27.33	5.58	14.96	2.05	12.24	1.76	137.30	573.30	4.55	3.70	2.26	1.45	0.14	0.76
H14	212.80	48.50	42.00	169.20	32.47	8.71	39.59	5.73	32.02	6.65	17.91	2.55	15.73	2.25	176.40	636.11	4.20	4.39	2.43	1.32	0.12	0.74
Average	152.19	35.16	32.96	137.35	24.85	6.33	28.13	4.55	24.47	4.56	13.48	1.71	10.88	1.53	132.41	478.15	4.35	4.33	2.14	1.46	0.12	0.73
A1	186.20	34.20	40.61	162.70	30.72	7.84	36.01	5.26	28.32	6.02	15.93	2.24	13.31	1.92	149.30	571.28	4.24	5.44	2.22	1.38	0.09	0.72
A2	176.80	40.70	37.83	147.30	28.62	7.22	31.52	4.80	25.68	5.12	13.94	1.96	11.63	1.61	126.70	534.73	4.56	4.34	2.32	1.43	0.12	0.73
A3	173.90	38.60	39.48	154.30	29.81	7.37	31.47	4.82	25.77	5.25	14.25	1.96	11.63	1.67	110.30	540.28	4.58	4.51	2.18	1.44	0.11	0.73
A4	143.20	32.80	32.40	129.60	25.19	6.53	28.70	4.28	22.43	4.73	12.65	1.76	10.23	1.45	105.60	455.95	4.29	4.37	2.14	1.42	0.12	0.74
A5	159.10	28.20	30.94	122.40	23.29	6.04	27.90	4.19	22.31	4.78	13.57	1.83	10.98	1.55	120.60	457.08	4.25	5.64	2.52	1.32	0.10	0.72
A6	151.10	42.30	33.17	127.00	25.27	6.47	28.83	4.37	23.62	5.03	13.80	1.93	11.07	1.66	122.50	475.62	4.27	3.57	2.30	1.38	0.14	0.73
Average	165.05	36.13	35.74	140.55	27.15	6.91	30.74	4.62	24.69	5.16	14.02	1.95	11.48	1.64	122.50	505.82	4.36	4.57	2.27	1.40	0.11	0.73
KM1	143.70	29.70	29.62	122.30	22.21	6.00	25.25	3.89	21.61	4.31	12.07	1.69	9.78	1.41	112.60	433.54	4.42	4.84	2.27	1.43	0.11	0.77
KM2	152.10	35.70	33.90	136.80	25.50	6.66	27.07	4.27	22.83	4.57	12.57	1.72	9.82	1.41	119.40	474.92	4.64	4.26	2.15	1.51	0.12	0.77
KM3	130.40	27.20	28.08	116.40	21.32	5.90	24.22	3.81	20.34	4.21	11.96	1.65	9.32	1.36	111.80	406.17	4.28	4.79	2.17	1.42	0.11	0.79
KM4	139.30	26.90	29.18	118.90	21.76	5.75	24.25	3.80	20.52	4.21	11.59	1.60	9.47	1.32	104.10	418.55	4.45	5.18	2.27	1.41	0.10	0.76
KM5	150.30	27.00	30.31	123.10	22.82	6.14	26.60	4.08	22.21	4.52	12.64	1.76	10.07	1.44	123.60	422.99	4.32	5.57	2.36	1.43	0.10	0.76
Average	143.16	29.30	30.22	123.50	22.72	6.09	25.48	3.97	21.50	4.36	12.17	1.68	9.69	1.39	114.30	435.23	4.42	4.89	2.24	1.44	0.11	0.77

to the low Cr concentrations, Ni content of ferromanganese ores is relatively high. This means that there is no leaching from ultramafic rocks, but again relatively high values of Ni may be an indicator of sulfide ores at depth.

According to Hein et al. (2008), high Cu, Zn, Pb, and Cd concentrations typically reflect the influence of sulfides, such as whether sulfides were precipitated at depth and if so whether they were later leached by the fluids that precipitated the Mn oxides. Copper and Pb concentrations in the ores range from 16.2 to 5448.3 ppm (average = 468) and 31.6 to 293 ppm (average = 140), respectively. Enrichment of Cu and Pb in ferromanganese ores may also provide evidence of leaching from sulfide mineralization at depth. High

Mo concentrations may reflect leaching only at high temperatures (i.e., >310 °C) in the hydrothermal fluids as well as leaching of acidic to mafic igneous rocks (Hein et al., 2008). Molybdenum concentrations in the ores range from 2.9 to 75.8 ppm (average = 13). Low Mo content in ferromanganese ores may reflect the low-temperature conditions of hydrothermal fluids. Hydrothermal oxides are lower in cobalt content when compared to hydrogenous deposits; high cobalt concentrations are indicative of marine environments (Del Rio Salas et al., 2008). Cobalt concentrations of Mn–Fe deposits in the Maden complex range from 32 to 99.10 ppm (average = 65.96) with the low Co content in ferromanganese ores suggesting a minimum hydrogenic contribution during mineralization. Hein et al. (2008) noted that high Ba and minor components of Fe, Co, Ni, Cu, and Zn concentrations in Mn oxides probably reflect either the leaching of organic-rich biogenic sediments or the lack of precipitation of barite at depth in the hydrothermal systems. Barium concentrations in hydrothermal solutions are higher than seawater because of the influence of volcanic activity and sedimentation (Monnin et al., 2001; Öksüz, 2011). Barium concentrations in the Maden complex ferromanganese deposits range from 15 to 41,213 ppm (average = 1690) reflecting in general, the characteristics of submarine hydrothermal deposits. A high arsenic content is diagnostic of hydrothermal manganese input to the sediments (Nicholson, 1992a,b). Arsenic enrichment in the studied ferromanganese samples ranges from 18.6 to 714.3 ppm (average = 205). These enrichments show a uniform trend (see Table 2) and may also be an indicator of hydrothermal fluids.

Trace element (i.e., As, Cu, Ni, Pb, Sr, V, and Zn) concentrations of ores in the Maden complex are generally low when compared with concentrations in hydrogenous deposits but are slightly higher with regard to hydrothermal deposits (see Table 3). Aluminium and Ti concentrations are used for the identification of manganese mineralization, and Al is generally related to clay minerals in the sediments (Crerar et al., 1982). Titanium is immobile in hydrothermal solutions and as such is measure of clastic input (Sugisaki, 1984). The relatively high concentrations of Al values in Mn oxide deposits also suggest a significant sedimentary contribution during precipitation (Choi and Hariya, 1992). Aluminium concentrations of ores in the Maden complex range from 0.40 to 4.76 wt.% (average = 2.36), and Ti concentrations range from 0.01 to 0.25 wt.% (average = 0.10) (see Table 1). The relatively high Al concentrations in the ores of Maden complex Mn–Fe deposits might result from mudstones, which are the host rocks of the ores. Low titanium values indicate limited clastic material entry during mineralization.

Different major and trace element discrimination diagrams have been proposed by many workers to distinguish manganese ores of various origins (Adachi et al., 1986; Bonatti et al., 1972; Choi and Hariya, 1992; Crerar et al., 1982; Nicholson, 1992a; Peters, 1988; Shah and Moon, 2007; Toth, 1980). These discrimination diagrams have been used to distinguish between a hydrothermal (continental or marine) and a hydrogenous origin. The term *hydrothermal* refers to manganese oxides deposited directly from geothermal waters around hot springs and pools in continental environments or sedimentary-exhalative manganese mineralization deposited in marine environments (Nicholson, 1992a and references therein). The term *hydrogenous* refers to deposits formed by slow precipitation or adsorption of dissolved components from seawater (Bonatti et al., 1972; Crerar et al,., 1982; Nicholson, 1992a).

The Mn–Fe–(Co + Ni + Cu) × 10 triangular diagram (Bonatti et al., 1972; Crerar et al., 1982), the Zn–Ni–Co triangular diagram (Choi and Hariya, 1992), and the Co:Zn vs. Co + Ni + Cu diagram (Toth, 1980) are used in this study to discriminate between the hydrothermal and hydrogenous character of the deposits. All the studied ferromanganese ore samples in triangular (Fig. 7A and B) and binary (Fig. 7C) discrimination diagrams plot within the hydrothermal field.

Trace element concentrations in the manganese oxides show the mostly hydrothermal origin for all ferromanganese deposits in the Elazığ–Malatya region (see Table 2; Fig. 7A–C). Table 3 shows the major and trace element abundances of various manganese deposits of hydrothermal and hydrogenous origins from Turkey and the world. The major and trace element concentrations of the Maden complex Mn–Fe deposits are comparable with those of the Koryu, Hinode, and Mn–Fe deposits of the Tokoro belt (Choi and Hariya, 1992) (see Table 3). The relationships between Mn and Fe are defined as Mn:Fe < 1 for a lacustrine environment, Mn:Fe = 1 for a hydrogenous origin, and 0.1 < Mn:Fe < 10 for SEDEX deposits. The Mn:Fe ratios of Maden complex Mn–Fe deposits range from 0.23 to 2.24 (average = 0.63), which are consistent with those of sedimentary-exhalative manganese deposits.

5.4. Rare earth elements in the manganese oxides

The analytical results of 56 selected ore samples from eight locations are listed in Table 4. Hydrothermal deposits show relatively low REE, but hydrogenous deposits have a significantly higher amount (Hein et al., 1990; Usui and Someya, 1997; see also Kato et al., 2011). Moreover, hydrothermal oxides have a wide range of total REE content (Mills et al., 2001). The total REE (ΣREE) concentrations of Maden complex Mn–Fe ores range from 64.39 to 738.23 ppm (average = 501.54), which are slightly higher than those of hydrothermal deposits but relatively lower than hydrogenous deposits. Although the Mn–Fe ores of the Maden complex are slightly enriched in REE (see Tables 4 and 5),

Table 5
REE concentrations (ppm) of hydrogenous and hydrothermal type manganese oxide deposits from different localities. Table also includes those of the Elazığ–Malatya region Mn–Fe deposits.

Locality	La	Ce	Pr	Nd	Sm	Eu	Gd	Tb	Dy	Ho	Er	Tm	Yb	Lu	∑REE	Deposit type	References
Indian Ocean	153.4	714.1	34.8	142.0	33.8	8.9	43.7	5.7	30.6	5.6	15.5	2.3	15.0	2.2	1207.6	Hydrogenous	Nath et al. (1992)
Johnston Island	260.0	1201.0	44.8	192.7	35.4	10.1	48.5	6.8	43.7	9.9	28.9	4.3	27.9	3.6	1917.7	Hydrogenous	Wiltshire et al. (1999)
Pitcairn Island hotspot	276.8	741.7	50.8	214.4	42.7	10.2	49.9	7.2	44.7	9.2	26.4	3.9	26.0	4.0	1508.1	Hydrogenous	Glasby et al. (1997)
Indian Ocean	183.2	163.8	–	164.4	35.3	9.1	37.2	–	34.7	–	–	–	17.6	2.6	647.9	Hydrothermal	Nath et al. (1997)
Pitcairn Island hotspot	33.8	48.3	9.9	39.1	8.4	2.5	7.5	1.1	6.4	1.1	3.2	0.4	2.6	0.4	164.9	Hydrothermal	Glasby et al. (1997)
Hydrothermal deposits (East Pasific Rise)	182.0	93.7	–	159.0	28.3	6.2	–	5.4	–	–	–	–	18.3	3.2	495.4	Hydrothermal	Piper and Graff (1974)
Neptuno deposit	125.2	289.3	24.4	78.7	12.8	7.2	10.3	1.3	6.6	1.1	3.1	0.3	2.3	0.3	563.1	Hydrothermal	Del Rio Salas (2008)
Baleo deposit	118.6	190.3	5.4	28.4	7.8	0.1	5.8	0.9	7.5	1.6	6.0	0.7	6.1	0.8	379.8	Hydrothermal	Del Rio Salas (2008)
Beyhan deposit	148.8	56.2	35.9	146.6	26.9	6.6	28.8	4.8	24.4	4.5	13.2	1.7	10.8	1.5	510.9		This study
Palu deposit	134.6	46.8	32.4	135.4	24.2	5.9	26.1	4.4	23.1	4.1	12.3	1.5	10.0	1.4	462.1		
Sarıkamış deposit	180.3	66.8	40.0	162.7	30.7	7.7	33.8	5.1	27.2	5.7	15.4	2.1	12.4	1.8	591.7		
Koçkale deposit	147.9	35.7	33.9	141.7	25.1	6.4	28.5	4.8	25.1	4.6	13.6	1.7	11.1	1.5	481.5		
Germili deposit	192.1	79.8	47.8	195.9	35.5	8.6	37.9	6.4	32.5	5.8	17.2	2.1	14.1	1.9	677.5		
Hazar deposit	152.2	35.2	33.0	137.4	24.8	6.3	28.1	4.6	24.5	4.6	13.5	1.7	10.9	1.5	478.2		
Alihan deposit	165.1	36.1	35.7	140.6	27.2	6.9	30.7	4.6	24.7	5.2	14.0	1.9	11.5	1.6	505.8		
Kom deposit	143.2	29.3	30.2	123.5	22.7	6.1	25.5	4.0	21.5	4.4	12.2	1.7	9.7	1.4	435.2		

the total REE concentrations are within the range of hydrothermal deposits (Hein et al., 1987). We note that a slight increase in the total REE concentrations of ferromanganese ores is due to the sedimentary cover.

Total light REE:heavy REE (i.e., ΣLREE:ΣHREE) and La:Ce ratios of the Maden complex Mn-Fe ores given in Table 4, can be used as an indicator of primary enrichment during the Mn oxidation processes (Öksüz, 2011; Xie et al., 2006). A LREE > HREE value may indicate mineralization related to hydrothermal solutions (Fitzgerald and Gillis, 2006; Öksüz, 2011). The total LREE:total HREE ratio ranges from 3.00 to 5.03 (average = 4.44) in the Maden complex Mn–Fe ores. These values indicate that hydrothermal solutions played an important role in the formation of Maden complex Mn–Fe deposits. Hydrothermal crusts have La:Ce ratios similar to seawater (~2.8), but hydrogenous Mn–Fe crusts have a much lower La:Ce ratio (~0.25) (Nath et al., 1997). La:Ce ratios for the Maden complex Mn–Fe ores vary between 0.82 and 6.25 (average 3.88) (see Table 4). This ratio suggests a major input from a hydrothermal source for the Maden complex Mn–Fe ores.

La_N:Nd_N and Dy_N:Yb_N ratios are 3.0–7.4 and 0.6–2.1 in hydrothermal solutions and 2.7–4.3 and 0.4–1.2 in Mn-oxide crusts, respectively (Fitzgerald and Gillis, 2006; Öksüz, 2011). La_N:Nd_N ratios range from 1.75 to 2.54 (average = 2.09), and Dy_N:Yb_N ratios range from 1.20 to 1.63 (average = 1.46) in the Maden complex Mn–Fe ores. Despite low La_N:Nd_N ratios, especially relatively high Dy_N:Yb_N ratios may indicate a hydrothermal origin for the formation of Maden complex Mn–Fe ores.

Although the relationship between manganese deposits and their REE distribution has been studied (Bender et al., 1971; Dymond et al., 1973; Graff, 1978; Haskin et al., 1966), there is no generally accepted model for reflecting the deposit type (e.g., hydrothermal, hydrogenetic, diaganetic) and oxidative and reductive deposition conditions. Cerium and europium, the two most important REEs, are commonly used for the prediction of fluid source and redox potential of the environment.

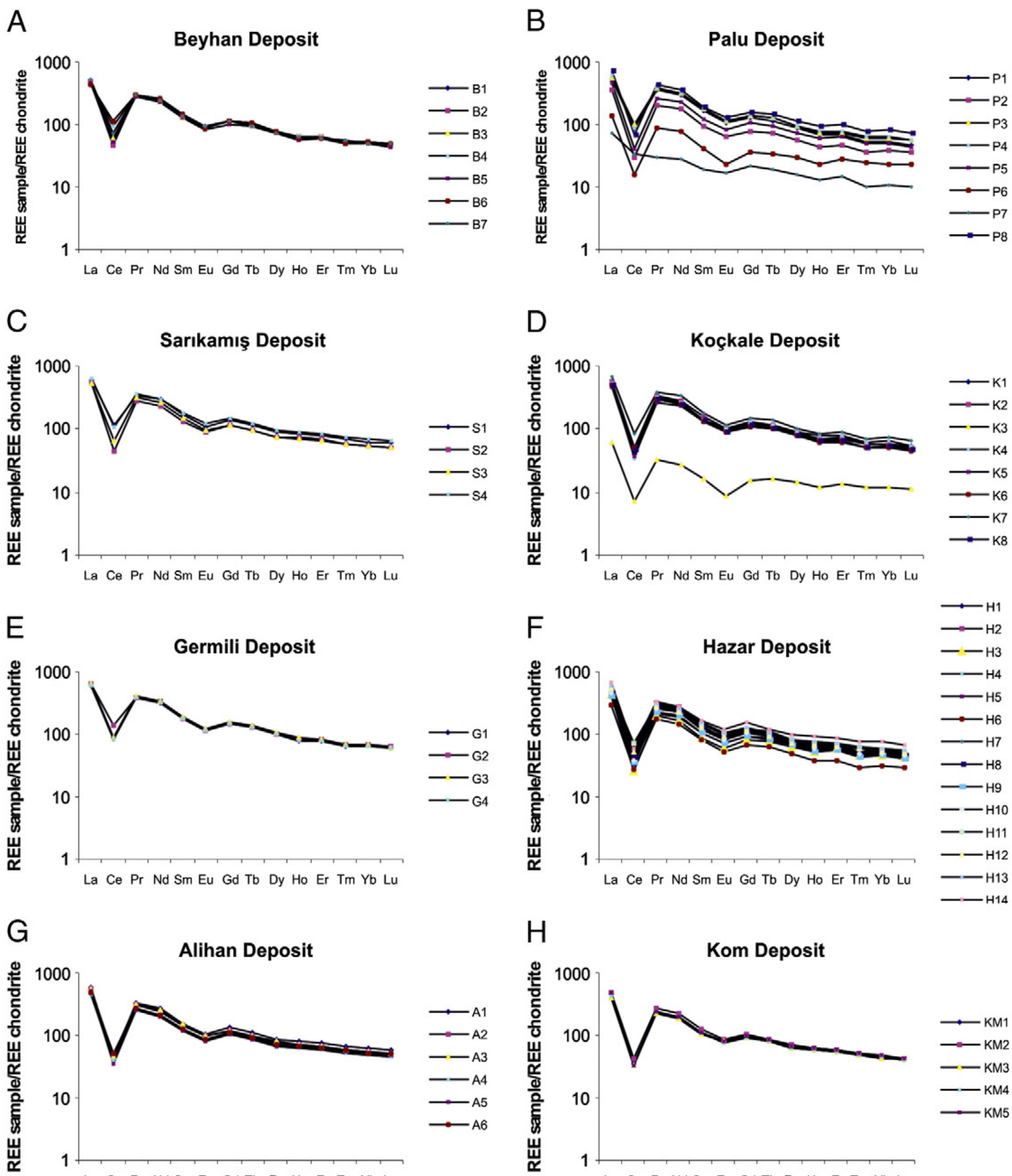

Fig. 8. Chondrite-normalized REE patterns for the Maden complex manganese deposits from Elazığ–Malatya region.

Slight negative Ce anomalies are considered as an indicator of volcanogenic input (Fleet et al., 1976) or hydrothermal contributions to seawater (Bender et al., 1971; Dymond et al., 1973), whereas a strong negative Ce anomaly is characteristic of low-temperature hydrothermal deposits around the hot spots in mid-ocean and island arc spreading centers (De Carlo and Mc Murtry, 1992; Hodkinson et al., 1994). Positive Ce anomalies are characteristic for modern sea-floor oxy-hydroxide deposits and nodules (Kunzendorf and Glasby, 1994). A negative Ce anomaly is observed in all ore samples taken from the Maden complex (see Table 4). Cerium anomaly values range between 0.08 and 0.72 (average = 0.15) a range which is similar to low-temperature hydrothermal deposits. A positive Eu anomaly in hydrothermal deposits suggests high-temperature hydrothermal fluids (Michard, 1989) and reflects the interaction of heated waters with substrate volcanic rocks of high Eu content during circulation (Usui and Mita, 1995). A negative Eu anomaly indicates an insufficient interaction of ground water with substrate volcanic rocks due to low temperature (Usui and Mita, 1995) and contamination from the continental crust and/or sediment contribution (Öksüz, 2011; Sun and McDonough, 1989). A negative Eu anomaly is found in all the ferromanganese samples taken from the Maden complex. Europium anomaly values range from 0.55 to 0.82 (average = 0.73). This suggests a low-temperature hydrothermal solution, which affected mineralization, and also indicates that there is insufficient interaction with the underlying volcanic rocks.

Cerium and Eu anomalies are defined as $Ce/Ce^* = [(Ce_N)/(La_N{}^*Pr_N)^{1/2}$ and $Eu/Eu^* = [(Eu_N)/(Sm_N{}^*Gd_N)^{1/2}$, respectively, where Ce^* and Eu^* are the hypothetical concentrations (Kato et al., 2006). The subscript "N" indicates chondrite-normalized values (Boynton, 1984). Ce/Ce^* and Eu/Eu^* values range from 0.08 to 0.72 (average = 0.15) and 0.55 to 0.82 (average = 0.73), respectively, in the Maden complex Mn–Fe ores (see Table 4). Ce/Ce^* values of Mn–Fe ores agree well with those of some deep-sea waters ($Ce/Ce^* = 0.03$–0.25; Kato et al., 2006) and Fe–Mn sediments ($Ce/Ce^* = 0.12$–0.26; Kato et al., 2006). Eu/Eu^* values of ores agree well with those of Fe–Mn sediments (0.75–0.93; Kato et al., 2006) but are slightly higher than those of deep-sea waters (0.63–0.72; Kato et al., 2006) because of the contribution of submarine hydrothermal fluids.

We conclude that the REE patterns of the Maden complex ferromanganese deposits are generally similar to those from hydrothermal manganese deposits. All the studied deposits show strong negative Ce and slight negative Eu anomalies (Fig. 8). This indicates that all the deposits were formed from reducing to suboxic solutions and also suggests an insufficient interaction of groundwater with substrate volcanic rocks due to low-temperature conditions. Submarine hydrothermal Fe–Mn sediments generally show remarkable depletion of Ce and less striking depletion of Eu in deep-sea water because of the scavenging of REEs from deep-ocean water (Balistrieri et al., 1981). REE patterns of the Maden complex ores are generally similar to the REE patterns of submarine hydrothermal deposits but differ from them as a result of a slightly higher REE content.

Table 5 shows REE abundances of various manganese oxide deposits of hydrothermal and hydrogenous origins. In comparison to the REE values in Table 5, the Maden complex deposits do not have the high Ce values of hydrogenous deposits and are more like hydrothermal deposits in this feature. The total REE content of the Mn–Fe ores from the Maden complex also confirms the hydrothermal nature of these deposits. The chondrite-normalized REE patterns of the Elazığ–Malatya region samples (Fig. 8) are generally similar to those of hydrothermal manganese deposits and have a hydrothermal character based on the discrimination diagrams of Bonatti et al. (1972), Toth (1980), Crerar et al. (1982), and Choi and Hariya (1992). A comparison of the graphs in Fig. 8 with those in Fig. 9 confirms that the Maden complex deposits were formed by hydrothermal processes. The Maden complex deposits do not exhibit the positive Ce spike of the hydrogenetic Mn crusts in Fig. 9E. Their REE profile closely resembles that of the Phanerozoic Fe–Mn umbers and less closely to that of EPR hydrothermal Fe–Mn sediments (Fig. 9C and 9D). Normalized REE patterns and REE concentrations are similar throughout all the deposits. Such similar REE characteristics among the eight deposits suggest that similar processes were operating during their formation. The K3 sample from Koçkale and the P7 sample from Palu display a

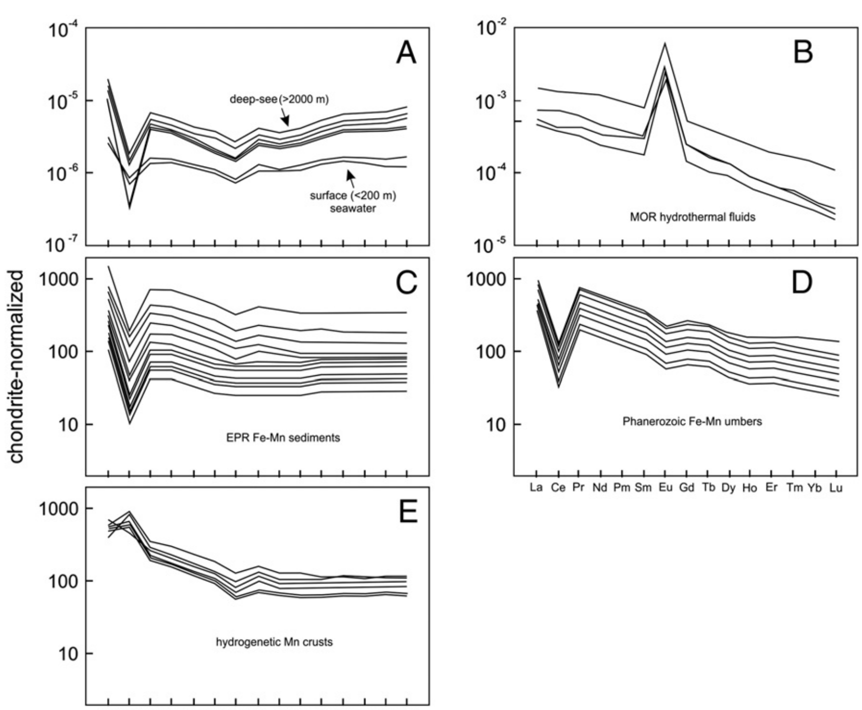

Fig. 9. (A) = Chondrite-normalized REE patterns of modern seawater, (B) = MOR hydrothermal fluids, (C) = EPR (East Pacific Rise) hydrothermal Fe–Mn sediments, (D) = Phanerozoic hydrothermal Fe–Mn umbers, and (E) = Hydrogenetic Mn crusts.
Taken from Kato et al. (2006).

relatively low chondrite-normalized REE pattern when compared to the other samples, probably due to the intensively altered specimens.

6. Conclusions

Mn–Fe deposits in the Maden complex are associated with the volcano-sedimentary Melafan formation, which was formed predominantly by red and dark purplish mudstones. The Melafan formation includes green spilitic basalt and diabase intercalations, especially in the lower part of the unit, with varying thicknesses of 30 cm to 30 m. Red and dark purplish radiolarites are also seen within the volcanic rocks. The Maden complex contains many Mn–Fe deposits that are hosted in mudstones; these deposits occur as lenses and thin layers. Lithological and geochemical characteristics suggest that the Maden complex rocks were deposited in a back-arc basin environment. The Mn–Fe mineralization of the Elazığ–Malatya region was influenced by basement structures, which relate to the opening of the Maden marginal basin. The mineralizing solutions ascended through these structures, as indicated by the presence of veinlets containing copper oxide minerals along the fractures of underlying spilitic basalt and diabase around the Elazığ–Malatya region. The Mn–Fe ore mineralogy, major, trace, and REE geochemistry support a hydrothermal origin. Magmatism during the evolution of the Maden marginal basin could have triggered the convection of geothermal water and promoted leaching of the spilitic basalt and diabase that resulted in the formation of Mn–Fe mineralization around the Elazığ–Malatya region. The ore deposition style is sedimentary exhalative. The features of the environment are suggested by the red mudstones and radiolarites associated with volcanic spilitic basalt and diabase rocks, Fe–Mn mineralization in lenses and stratiform layers, widespread copper oxide minerals in volcano-sedimentary rocks, a conformable relation with wall rocks, lack of alteration in wall rocks, mineralogy of ore minerals, and hydrothermal characteristics of ore-forming fluids.

Acknowledgments

This work has been funded by both TUBITAK, the Scientific and Technical Research Council of Turkey (Project No. TÜBİTAK 106Y061) and the Firat University Scientific Research Project Foundation (FUBAP-553). We thank the anonymous reviewers for their constructive comments, which significantly improved the manuscript. We also thank Editor-in-Chief Franco Pirajno for his valuable contributions during the editorial handling of the manuscript.

References

Açıkbaş, D., Baştuğ, C., 1975. V. Bölge Cacas-Hani yöresi kuzey sahalarının jeoloji raporu ve petrol olanakları. Yayımlanmamış rapor, Türkiye Petrolleri Anonim Ortaklığı (TPAO); 917, Ankara, Türkiye.

Adachi, M., Yamamoto, K., Sugisaki, R., 1986. Hydrothermal chert and assoicated siliceous rocks from the northern Pasific: their geological significance as indication of ocean ridge activity. Sediment. Geol. 47, 125–148.

Akıncı, Ö.T., 2009. Ophiolite-hosted copper and gold deposits of southeastern Turkey: formation and relationship with seafloor hydrothermal processes. Turk. J. Earth Sci. 18, 475–509.

Aktaş, G., Robertson, A.H.F., 1984. The Maden Complex, SE Turkey: evolution of a Neotethyan continental margin. In: Dixon, J.E., Robertson, A.H.F. (Eds.), The geological evolution of the eastern Mediterranean. Geological Society Special Publications, London, 17, pp. 375–402.

Aktaş, G., Robertson, A.H.F., 1990. Tectonic evolution of the Tethys suture zone in SE Turkey: evidence from the petrology and geochemistry of Late Cretaceous and Middle Eocene extrusives. In: Moores, E.M., Panayiotou, A., Xenophontos, C. (Eds.), Ophiolites-Oceanic Crustal Analogues. Proceedings International Symposium "Trodos 1987". Geological Survey Department, Nicosia, pp. 311–329.

Altunbey, M., Sağıroğlu, A., 1995. Koçkale-Elazığ manganez cevherleşmelerinin özellikleri ve kökeni. Maden Tetkik ve Arama Genel Müdürlüğü (MTA) Dergisi 117, 139–148.

Balistrieri, L.S., Brewer, P.G., Murray, J.W., 1981. Scevenging residence times and surface chemistry. Deep-Sea Res. 28A, 101–121.

Bamba, T., 1973. Kısabekir-Maden-Hacan bakır sahalarında 1972 yılında yapılan çalışmalara ait rapor. Yayımlanmamış rapor, Maden Tetkik ve Arama Genel Müdürlüğü (MTA); 4953, Ankara, Türkiye.

Bamba, T., 1976. Güneydoğu Anadolu Ergani-Maden bölgesi ofiyolit ve ilgili bakır yatağı. Maden Tetkik ve Arama Genel Müdürlüğü (MTA) Dergisi 86, 35–49.

Bamba, T., Tin, A., 1972. Ergani-Maden bölgesinin bakır yatakları, güneydoğu Türkiye. Yaımlanmamış rapor. Maden Tetkik ve Arama Genel Müdürlüğü (MTA), 4968 (Ankara, Türkiye).

Bender, M.L., Broecker, W., Gornitz, V., Middel, U., Kay, R., Sun, S.S., Biscaye, P., 1971. Geochemistry of three cores from the East Pasific Rise. Earth Planet. Sci. Lett. 12, 425–433.

Bonatti, E., Kraemer, T., Rydel, H., 1972. Classification and genesis of submarine iron–manganese deposits. In: Horn, D.R. (Ed.), Ferromanganese Deposits on the Ocean Floor, Washington, D. C., Natl. Sci. Found, pp. 149–166.

Borchert, H., 1952. Ergani bakır cevheri yataklarında yapılan jeolojik tatbikata ait rapor. Yayımlanmamış rapor, Maden Tetkik ve Arama Genel Müdürlüğü (MTA), 2083, Ankara, Türkiye.

Boynton, W.V., 1984. Geochemistry of the rare earth elements: meteorite studies. In: Henderson, P. (Ed.), Rare Earth Element Geochemistry. Elsevier, pp. 63–114.

Bozkaya, Ö., Yalçın, H., Dündar, M.K., 2006. Maden Grubu (Malatya–Pütürge) kayaçlarında diyajenez/metamorfizma ve jeotektonik konum arasındaki ilişkiler. Cumhuriyet Üniversitesi Mühehdislik Fakültesi Dergisi, Seri A, Yerbilimleri 23 (1-2), 1–24.

Bozkurt, E., 2001. Neotectonics of Turkey—a synthesis. Geodin. Acta 14, 3–30.

Choi, J.H., Hariya, Y., 1992. Geochemistry and depositional environment of Mn oxide deposites in the Tokora Belt, norteastern Hokkaido, Japan. Econ. Geol. 87, 1265–1274.

Crerar, D.A., Namson, J., Chyi, M.S., Williams, L., Feigenson, M.D., 1982. Manganiferous cherts of the Franciscan assemblage: I. General geology, ancient and modern analogues, and implications for the hydrothermal convection at oceanic spreading centers. Econ. Geol. 77, 519–540.

De Carlo, E.H., McMurtry, G.M., 1992. Rare earthelement geochemistry of ferromanganese crusts from the Hawaiilan Archi-pelago, central Pasific. Chem. Geol. 95, 235–250.

Del Rio Salas, R., Ruiz, J., Ochoa-Landin, L., Noriega, O., Bara, F., Meza-Figueroa, D., Paz-Moreno, F., 2008. Geology, geochemistry and Re–Os systematics of manganese deposits from the Santa Rosalia Basin and adjacent areas in Baja California Sur, Mexico. Miner. Deposita 43, 467–482.

Delian, F., 1994. Geological and Geochemical Research of the Manganese ore Bed (in Chinese), M1. Weather Publishing Press, Beijing.

Dymond, J., Corliss, J.B., Health, G.B., Field, C.W., Dash, E.J., Weeh, H.H., 1973. Origin of metalliferous sediments from the Pasific Ocean. Geol. Soc. Am. Bull. 84, 3355–3372.

Elitok, Ö., Dolmaz, M.N., 2011. Tectonic escape mechanism in the crustal evolution of eastern Anatolian region (Turkey). In: Schattner, Uri (Ed.), At the Midst of Plate Convergence. ISBN: 978-953-307-594-5, pp. 289–302.

Elmas, A., Yılmaz, Y., 2003. Development of an oblique subduction zone-tectonic evolution of the Tethys suture zone in southeast Turkey. Int. Geol. Rev. 45, 827–840.

Emin, C., 1979. Malatya ili, Pütürge ilçesi, Çanakçı köyü sahasının jeoloji raporu. Yayımlanmamış rapor, Maden Tetkik ve Arama Genel Müdürlüğü (MTA), 6577, Ankara, Türkiye.

Erdoğan, B., 1977. Geology, Geochemistry and Genesis of the Sulphide Deposit, of the Ergani–Maden Region, SE Turkey. (PhD thesis) New Brunswick University, New Brunswick (249 pp.).

Erdoğan, B., 1982. Geology and volcanic rocks of the southeast Anatolian ophiolite belt of the Ergani–Maden region. Bull. Geol. Soc. Turk. 25, 49–59.

Erler, A., 1983. Tectonic setting of the massive sulphide deposit of the Southeast Anatolian thrust belt. In: Tekeli, O., Göncüoğlu, M.C. (Eds.), Geology of the Taurus Belt. General Directorate of Mineral Research and Exploration (MTA), Ankara, pp. 309–316.

Fernandez, A., Moro, M.C., 1998. Origin and depositional environment of Ordovician stratiform iron mineralization from Zamora (NW Iberian Peninsula). Miner. Deposita 33, 606–619.

Fitzgerald, C.E., Gillis, K.M., 2006. Hydrothermal manganese oxide deposits from Baby Bare seamount in the Northeast Pacific Ocean. Mar. Geol. 225, 145–156.

Fleet, H.J., Henderson, P., Kepme, D.D.C., 1976. Rare earth element and related chemistry of some drilled Southern Indian Ocean basalts and volcanogenic sediments. J. Geophys. Res. (JGR) 81, 4257–4268.

Gedikoğlu, A., Van, A., Eyüpoğlu, I., Yalçınalp, B., 1985. Doğu Karadeniz cevherleşmelerine bir örnek: Ocaklı (Maçka–Trabzon) manganez zuhuru. Jeoloji Mühendisliği Dergisi 25, 23–37.

Glasby, G.P., Stüben, D., Jeschke, G., Stoffers, P., Garbe-Schönberg, C.D., 1997. A model for the formation of hydrothermal manganese crusts from the Pitcairn Island hotspot. Geochim. Cosmochim. Acta 61, 4583–4597.

Göncüoğlu, M.C., Dirik, K., Kozlu, H., 1997. Pre-Alpine and Alpine terranes in Turkey: explanatory notes to the terrane map of Turkey. Ann. Géol. Pays Hellén. 37, 515–536.

Göymen, G., Aslaner, M., 1969. Doğu Anadolu'da bulunan Ergani–Maden bakır yatağının ve bilhassa yantaşlarının maden mikroskopik incelenmesi. Maden Tetkik ve Arama Genel Müdürlüğü (MTA) Dergisi 72, 176–188.

Graff, J.L., 1978. Rare earth elements in iron formations and sea water. Geochim. Cosmochim. Acta 42, 1845–1850.

Griffits, W.R., Albers, J.P., Öner, Ö., 1972. Massive sulphide copper deposits of the Ergani–Maden area, southeastern Turkey. Econ. Geol. 67, 701–713.

Gültekin, A.H., 1998. Geochemistry and origin of the Oligocene Binkılıç manganese deposit, Thrace basin, Turkey. Turk. J. Earth Sci. 7, 11–24.

Gürbüz, K., Gül, M., 2005. Evolution of and factors controlling Eocene sedimentation in the Darende Balaban basin, Malatya (Eastern Turkey). Turk. J. Earth Sci. 14, 311–355.

Gürocak, Z., 1992. Sivrice (Elazığ) çevresinin jeolojisi. (Yüksek Lisans Tezi) Elazığ; Fırat Üniversitesi, Fen Bilimleri Enstitüsü (65 s).

Haskin, L.A., Frey, F.A., Schmitt, R., Smith, R.H., 1966. Meteoritic, solar and terrestrial rare earth distributions. Phys. Chem. Earth. 7, 167–321.

Hein, J.R., Koski, R.A., Yeh, H.W., 1987. Chert-hosted manganese deposits in sedimentary sequences of the Franciscan Complex, Diablo Range, California. In: Hein, J.R. (Ed.), Siliceous Sedimentary Rock-Hosted Ores and Petroleum. Van Nostrand Reinhold, New York, pp. 206–230.

Hein, J.R., Schulz, M.S., Kang, J.K., 1990. Insular and submarine ferromanganese mineralization of the Tonga-Lau region. Mar. Min. 9, 305–354.

Hein, J.R., Schulz, M.S., Dunham, R.E., Stern, R.J., Bloomer, S.H., 2008. Diffuse flow hydrothermal manganese mineralization along the active Mariana and southern Izu-Bonin arc system, western Pasific. J. Geophys. Res. 113, B08S14. http://dx.doi.org/10.1029/2007JB005432.

Helke, A., 1938. Elazığ vilayetindeki silisli demir-manganez cevherleri. Yayımlanmamış rapor, Maden Tetkik ve Arama Genel Müdürlüğü (MTA), 499, Ankara, Türkiye.

Helke, A., 1961. Beitrag zur Kenntnis der Chromerzlagerstâtten des Sori Dağı in der Türkei. N. Jahrb. Mineral. (Abh) 96, 48–78.

Hempton, M.R., 1984. Results of detailed mapping near Lake Hazar (Eastern Taurus Mountains). In: Tekeli, O., Göncüoğlu, M.C. (Eds.), Geology of the Taurus Belt. Proceedings of the International Symposium, 26–29 September 1983. General Directorate of Mineral Research and Exploration (MTA), Ankara, Turkey, pp. 223–228.

Hempton, M.R., 1985. Structure and deformation history of the Bitlis suture near Lake Hazar, SE Turkey. Geol. Soc. Am. Bull. 96, 223–243.

Hempton, M.R., Savcı, G., 1982. Petrological and structural features of the Elazığ volcanic complex. Bull. Geol. Soc. Turk. 25 (2), 143–151.

Hewett, D.F., Fleischer, M., 1960. Deposits of the manganese oxides. Econ. Geol. 55, 1–55.

Hodkinson, R.A., Stoffers, P., Scholten, P., Cronan, D.S., Jeschke, G., Rogers, T.D.S., 1994. Geochemistry of hydrothermal manganese deposits from the Pitcairn Island hotspot, southeastern Pasific. Geochim. Cosmochim. Acta 58, 5011–5029.

İleri, S., Salancı, B., Bitem, M., Doğan, R., 1976. Ergani (Maden) copper deposit and plate tectonics. Bull. Geol Soc. Turk 19, 133–142.

Karaman, T., Aslan, F., Bakırhan, B., Poyraz, N., Alan, İ., Kadınkız, G., Kılınç, F., Yılmaz, H., 1993. Malatya, Doğanşehir, Çelikhan dolaylarının jeolojisi. Yayımlanmamış rapor, Maden Tetkik ve Arama Genel Müdürlüğü (MTA); 9587, Ankara, Türkiye.

Kato, Y., Yamaguchi, K.E., Ohmoto, H., 2006. Rare earth elements in Precambrian banded iron formations: secular change of Ce and Eu anomalies and evolution of atmospheric oxygen. Geol. Soc. Amer. Mem. 198, 269–289.

Kato, Y., Fujinaga, K., Nakamura, K., Takaya, Y., Kitamura, K., Ohta, J., R., Toda, Nakashima, T., Iwamori, H., 2011. Deep-sea mud in the Pasific Ocean as a potential resource for rare-earth elements. Nat. Geosci. 4, 535–539.

Kaya, A., 2004. Gezin (Maden-Elazığ çevresinin jeolojisi. Pamukkale Üniversitesi, Mühendislik Fakültesi, Mühendislik Bilimleri Dergisi 10 (1), 41–50.

Ketin, İ., 1948. Ergani-Eğil bölgesinin (Pafta 80/4 ve 81/3) jeolojik etüdü hakkında memurat. Yayımlanmamış rapor, Maden Tetkik ve Arama Genel Müdürlüğü (MTA), 2015, Ankara, Türkiye.

Koç, S., Özmen, Ö., Öksüz, N., 2000. Kasımağa (Keskin-Kırıkkale) mangan oksit cevherleşmesinin oluşum ortamını tanımlayan jeokimyasal özellikler. Maden Tetkik ve Arama (MTA) Dergisi 122, 107–118.

Kovenko, V., 1943. Guleman madeninin simal, simal-doğu ve doğusundaki bölgenin istikşafı hakkında rapor. Yayımlanmamış rapor, Maden Tetkik ve Arama Genel Müdürlüğü (MTA), 1409, Ankara, Türkiye.

Kovenko, V., 1944. Elazığ-Ergani-Diyarbakır bölgesinin istikşafı hakkında rapor. Yayımlanmamış rapor, Maden Tetkik ve Arama Genel Müdürlüğü (MTA), 1947, Ankara, Türkiye.

Kunzendorf, H., Glasby, G.P., 1994. Minör and rare earth elements in manganese crusts and nodules and sediments from the Manihiki Plateau and adjacent areas: results of HMNZS Tui Cruises. Mar. Georesour. Geotechnol. 12, 271–281.

Kuşçu, M., Gedikoğlu, A., 1989. Ulukent (Tavas-Denizli) güneyi manganez yataklarının jeokimyasal özellikleri. Yerbilimcinin Sesi 17, 29–47.

Maynard, J.B., 2003. Chapter 15: manganiferous sediments, rocks, and ores. In: MacKenzie, F.T. (Ed.), Diagenesis, and Sedimentary Rocks. Treatise of Geochemistry, vol. 7. Elsevier, Amsterdam, pp. 289–308.

Maynard, J.B., 2010. The chemistry of manganese ores through time: a signal of increasing diversity of earth-surface environments. Econ. Geol. (Spec. Issue) 105 (3), 535–552.

Michard, A., 1989. Rare earth element systematics in hydrothermal fluids. Geochim. Cosmochim. Acta 53, 745–750.

Michard, A., Whitechurch, H., Ricou, L.E., Montigny, R., Yazgan, E., 1984. Tauric subduction (Malatya-Elazığ provinces) and its bearing on tectonics of the Tethyan realm in Turkey. In: Dixon, J.E., Robertson, A.H.F. (Eds.), The Geological Evolution of the Eastern Mediterranean. Geological Society, London, Special Publications, 17, pp. 361–374.

Michard, A., Juteau, T., Whitechurch, H., 1985. L'obduction; revue des modeles et confrontation au cas de l'Oman. Bull. Soc. Geol. Fr. 2, 189–198.

Mills, R.A., Wells, D., Roberts, S., 2001. Genesis of ferromanganese crusts from the TAG hydrothermal field. Chem. Geol. 176, 3–293.

Mineral Research and Exploration (MTA), 2002. 1/500.000 scale geological maps of Turkey. General Directorate of Mineral Research and Exploration (MTA), Ankara, Turkey.

Mohr, M., 1964. Elazığ havalisinde Muhittin Sabuncu'ya ait bazı maden zuhurları hakkında rapor. Maden Tetkik ve Arama Genel Müdürlüğü (MTA) yayını, 3348 (Ankara, Türkiye).

Monnin, C., Wheat, C.G., Dupre, B., Elderfield, H., Mottl, M.J., 2001. Barium geochemistry in sediment pore waters and formation waters of the oceanic crust on the eastern flank of the Juan de Fuca Ridge (ODP Leg 168). Geochem. Geophys. Geosyst. 2 (1), 1008 (15 pp.).

Nath, B.N., Balaram, V., Sudhakar, M., Plüger, W.L., 1992. Rare earth element geochemistry of ferromanganese deposits of the Indian Ocean. Mar. Chem. 38, 185–208.

Nath, B.N., Plüger, W.L., Roelandts, I., 1997. Geochemical constraints on the hydrothermal origin of ferromanganese encrustations from the Rodriguez Triple Junction, Indian Ocean. In: Nicholson, K., Hein, J.R., Bühn, B., Dasgupta, S. (Eds.), Manganese mineralization: Geochemistry and mineralogy of terrestrial and marine deposits. Geol. Soc. Spl. Pub., 119, pp. 199–211.

Nicholson, K., 1992a. Contrasting mineralogical–geochemical signatures of manganese oxides: quides to metallogenesis. Econ. Geol. 87, 1253–1264.

Nicholson, K., 1992b. Genetic types of manganese oxide deposits in scotland: Indicators of paleoocean-spreading rate and a Devonian geochemical mobility bondary. Econ. Geol. 87, 1301–1309.

Nicholson, K., Nayak, V.K., Nanda, J.K., 1997. Manganese ores of the Ghoriajhor-Monmunda area, Sundergarh District, Orissa, India: geochemical evidence for a mixed Mn source. In: Nicholson, K., Hein, J.R., Bühn, B., Dasgupta, S. (Eds.), Manganese mineralization: Geochemistry and Mineralogy of Terrestrial and Marine Deposits. Geological Society, Special Publication, London, 119, pp. 117–121.

Nurlu, N., 2009. İspendere ofiyolitinin kökensel incelenmesi. (Yüksek Lisans Tezi) Adana; Çukurova Üniversitesi, Fen Bilimleri Enstitüsü (105 s.).

Öksüz, N., 2011. Geochemical characteristics of the Eymir (Sorgun-Yozgat) manganese deposits, Turkey. J. Rare Earths 29 (3), 287–296.

Önal, A., Bingöl, A.F., 1997. Doğanşehir (Malatya) batısının jeolojisi. Selçuk Üniversitesi, Mühendislik Mimarlık Fakültesi Dergisi 12, 63–75.

Önal, Al., Şaşmaz, A., Önal, A., 2001. Alihan (Pütürge-Malatya) demirli manganez cevherleşmesinin mineralojik ve jeokimyasal özellikleri. 54. Türkiye Jeoloji Kurultayı Bildiri Özleri, JMO yayını, pp. 1–14 (Ankara, Türkiye).

Oygür, V., 1990. Çayırlı (Ankara-Haymana) manganez yatağının jeolojisi ve kökeni üzerine görüşler. Maden Tetkik ve Arama Genel Müdürlüğü (MTA) Dergisi 110, 29–44.

Özçelik, M., 1985. Malatya güneydoğusundaki Maden magmatik kayaçlarının jeolojisi ve tektonik ortamına jeokimyasal bir yaklaşım. Türkiye Jeoloji Kurumu Bülteni 28, 19–34.

Özkaya, İ., 1974. Sason-Baykan arasının stratigrafisi, güneydoğu Türkiye. Türkiye Jeoloji Kurumu Bülteni 17, 51–72.

Özkaya, İ., 1978. Yüksekova-Şemdinli yöresi stratigrafisi, tektonik evrimi ve petrol olanakları, Hakkari. (Doçentlik tezi) Orta Doğu Teknik Üniversitesi, Ankara (330 s).

Öztürk, H., 1993. Türkiye manganez yatakları: oluşumları ve tipleri. Jeoloji Mühendisliği Dergisi 43, 24–33.

Perinçek, D., 1978. Çelikhan-Sincik-Koçali (Adıyaman ili) alanının jeoloji incelemesi ve petrol olanaklarının araştırılması. (Doktora tezi) İstanbul Üniversitesi, İstanbul (212 s).

Perinçek, D., Özkaya, I., 1981. Arabistan levhası kuzey kenarı tektonik evrimi. Yerbilimleri Dergisi 8, 91–102.

Peters, T., 1988. Geochemistry of manganese-bearing cherts assoicated with Alpine-ophiolites and the Hawasina formations in Oman. Mar. Geol. 84 (3–4), 229–238.

Piper, D.Z., Graef, P.A., 1974. Gold and rare earth elements in sediments from the East Pacific rise. Mar. Geol. 17, 287–297.

Rigo de Righi, M., Cortesini, A., 1964. Gravity tectonics in foothills structure belt of southeast Turkey. Am. Assoc. Pet. Geol. Bull. 48, 1911–1937.

Rızaoğlu, T., Parlak, O., Hoeck, V., İşler, F., 2006. Nature and significance of Late Cretaceous ophiolitic rocks and their relaton to the Baskil granitic intrusions of the Elazığ region, SE Turkey. In: Robertson, A.H.F., Mountrakis, D. (Eds.), Tectonic Development of the Eastern Mediterranean Region. Geological Society, London, Special Publications, 260, pp. 327–350.

Robertson, A.H.F., 2000. Mesozoic-Tertiary tectonic-sedimentary evolution of a South Tethyan oceanic basin and its margins in southern Turkey. In: Bozkurt, E., Winchester, J.A., Piper, J.D.A. (Eds.), Tectonics and Magmatism in Turkey and the Surrounding Area. Geological Society, London, Special Publications, 173, pp. 43–82.

Robertson, A.H.F., Dixon, J.E., 1984. Introduction: aspects of the geological evolution of the Eastern Mediterranean. In: Dixon, J.E., Robertson, A.H.F. (Eds.), The Geological Evolution of the Eastern Mediterranean. Geological Society, London, Special Publications, 17, pp. 1–74.

Robertson, A.H.F., Parlak, O., Rızaoğlu, T., Ünlügenç, Ü., İnan, N., Taslı, K., Ustaömer, T., 2007. Tectonic evolution of the South Tethyan ocean: evidence from the Eastern Taurus Mountains (Elazığ region, SE Turkey). In: Ries, A.C., Butler, R.W.H., Graham, R.H. (Eds.), Deformation of the Continental Crust: The Lagacy of Mike Coward. Geological Society, London, Special Publications, 272, pp. 231–270.

Roy, S., 1992. Environments and processes of manganese deposition. Econ. Geol. 87, 1218–1236.

Roy, S., 1997. Genetic diversity of manganese deposition in the terrestrial geological record. In: Nicholson, K., Hein, J.R., Buhn, B., Dasgupta, S. (Eds.), Manganese Mineralization: Geochemistry and Mineralogy of Terrestrial and Marine Deposits. Geological Society, London, Special Publication, 119, pp. 5–27.

Schneiderhöhn, H., 1954. Ergani bakır yatağı, Yayımlanmamış rapor, Etibank Genel Müdürlüğü, 812, Ankara, Türkiye, 48 s.

Şengör, A.M.C., Yılmaz, Y., 1981. Tethyan evolution of Turkey: a plate tectonic approach. Tectonophysics 75, 181–241.

Shah, M.T., Moon, C.J., 2007. Manganese and ferromanganese ores from different tectonic settings in the NW Himalayas, Pakistan. J. Asian Earth Sci. 29, 455–465.

Sirel, M.A., 1949. Die Kupferlagerstaette Ergani-Maden in der Turkei. N. Jh. Mineral. Abh. Abt. A. 80, 36–95.

Sirel, M.A., 1952. Die Kupfererzlagerstaette Ergani Maden in der Türkei. N. Jb. Mineral. Abh. 80, 36–100 (Abt. A).

Sugisaki, R., 1984. Relation between chemical composition and sedimentation rate of Pacific ocean floor sediments deposited since the middle Cretaceous: basic evidence for chemical constraints on depsitional environments of ancient sediments. J. Geol. 92, 235–259.

Sun, S.S., McDonough, W.F., 1989. Chemical and isotopic systematics of oceanic basalts: implications for mantle compositions and processes. In: Saunders, A.D., Norry, M.J. (Eds.), Magmatism in the Ocean Basins. Geological Society, Special Publication, pp. 313–345.

Sungurlu, O., 1975. VI. Bölge kuzey sahalarının jeolojisi. Yayımlanmamış rapor, Türkiye Petrolleri Anonim Ortaklığı (TPAO), 817, Ankara, Türkiye.

Takashima, N., 1975. Ergani ve Madenköy Siirt ili arasındaki ofiyolit kuşağında zuhur eden bakır cevherleşmeleri. Yayımlanmamış rapor, Maden Tetkik ve Arama Genel Müdürlüğü (MTA), 5471, Ankara, Türkiye.

Toth, J.R., 1980. Deposition of submarine crusts rich in manganese and iron. Geol. Soc. Am. Bull. 91, 44–54.

Turan, M., Aksoy, E., Bingöl, A.F., 1995. Doğu Toroslar'ın Jeodinamik evriminin Elazığ civarındaki özellikleri. Fırat Üniversitesi, Fen ve Mühendislik Bilimleri Dergisi 7 (2), 177–199.

Türkyılmaz, B., 2004. Güneydoğu Anadolu Bindirme Kuşağındaki mangan yataklarının mineralojik, jeokimyasal ve kökensel olarak incelenmesi. (Doktora Tezi) Fırat Üniversitesi, Elazığ (160 s.).

Usui, A., Mita, N., 1995. Geochemistry and mineralogy of a modern buserite deposit from a hot spring in Hokkaido, Japan. Clays Clay Miner. 43 (1), 116–127.

Usui, A., Someya, M., 1997. Distribution and composition of marin hydrogenetic and hydrothermal manganese deposits in the North-west Pasific. In: Nicholson, K., Hein, J.R., Buhn, B., Dasgupta, S. (Eds.), Manganese Mineralization: Geochemistry and Mineralogy of Terrestrial and Marine Deposits. Geol. Soc. Lond. Spec. Publ., 119, pp. 177–198.

Wijkerslooth, P., 1943. Ergani-Maden bakır zuhuratının primer mineralleri. Maden Tetkik ve Arama Genel Müdürlüğü (MTA) Dergisi 31, 66–78.

Wijkerslooth, P., 1944. Elazığ ili (Ergani-Maden) bakır yatakları hakkındaki bilgiye yeni bir ilâve. Maden Tetkik ve Arama Genel Müdürlüğü (MTA) Dergisi 33, 76–104.

Wiltshire, J.C., Wen, X.Y., Yao, D., 1999. Ferromanganese crusts near Johnston Island: geochemistry, stratigraphy and economic potential. Mar. Georesour. Geotechnol. 17, 257–270.

Xie, J.C., Yang, X.Y., Du, J.G., Xu, W., 2006. Geochemical characteristics of sedimentary manganese deposit of Guichi, Anhui Province, China. J. Rare Earths 24 (3), 374–380.

Yazgan, E., 1972. Etude géologique et pétrographique du complexe ophiolitique de la région située au Sud-Est de Malatya (Taurus oriental, Turquie) et de sa couverture volcano-sédimentaire. (PhD these) Univ. de Genève; Département de minéralogie et géophysique, Geneve (236 pp.).

Yazgan, E., 1981. Doğu Toroslarda etkin bir paleo-kıta kenarı etüdü (Üst Kretase-Orta Eosen), Malatya-Elazığ, Doğu Anadolu. Hacettepe Üniversitesi Yer Bilimleri Dergisi 7, 83–104.

Yazgan, E., 1983. A geotraverse between the Arabian Platform and the Munzur Nappes. International Symposium on the Geology of the Taurus Belt, Guide Book for Excursion V., Ankara (17 pp.).

Yazgan, E., 1984. Geodynamic Evolution of the Eastern Taurus Region: Proceedings of International Symposium on the Geology of the Taurus Belt, Ankara. 199–208.

Yazgan, E., Chessex, R., 1991. Geology and tectonic evolution of southeastern Taurus in the region of Malatya. Turk. Assoc Pet. Geol. Bull 3, 1–42.

Yazgan E., Asutay, J., Gültekin, M.C., Poyraz, N., Yıldırım, H., 1986. 1:100.000 ölçekli Türkiye jeoloji Haritası Serisi, Malatya İ27 paftası. Maden Tetkik ve Arama Genel Müdürlüğü (MTA), Jeoloji Etüdleri Dairesi, Ankara, Türkiye.

Yazgan, E., Asutay, J., Gültekin, M.C., Poyraz, N., Sirel, E., Yıldırm, H., 1987. Malatya güneydoğusunun jeolojisi ve Doğu Torosların jeodinamik evrimi. Yayımlanmamış rapor, Maden Tetkik ve Arama Genel Müdürlüğü (MTA), 2268, Ankara, Türkiye.

Yiğitbaş, E., Yılmaz, Y., 1996a. New evidence and solution to the Maden complex controversy of the southeast Anatolian orogenic belt (Turkey). Geol. Rundsch. 85, 250–263.

Yiğitbaş, E., Yılmaz, Y., 1996b. Post-Late Cretaceous strike-slip tectonics and its implications on the Southeast Anatolian orogen, Turkey. Int. Geol. Rev. 38 (9), 818–831.

Yiğitbaş, E., Genç, Ş.C., Yılmaz, Y., 1993. Güneydoğu Anadolu orojenik kuşağında Maden grubunun tektonik konumu ve jeolojik önemi. In: Suat Erk, A. (Ed.), Jeoloji Simpozyumu Bildirileri, A.Ü Fen Fakültesi Jeoloji Mühendisliği Bölümü, Ankara, s, pp. 251–264.

Yıldırım, M., Yılmaz, Y., 1991. Güneydoğu Anadolu orojenik kuşağının ekaylı zonu. Türkiye Petrol Jeologları Derneği Bülteni (TPJD) 3, 57–73.

Yılmaz, O., 1971. Etude pétrographique et géochronologique de la région de Cacas. (Ph.D. thesis) Université Science et Médicale de Grenoble, Geneve (230 pp.).

Yılmaz, Y., 1993. New evidence and model on the evolution of the southeast Anatolian orogen. Geol. Soc. Am. Bull. 105, 251–271.

Yılmaz, H., 1999. Doğu Toroslarda Sürgü (Doğanşehir-Malatya) çevresinin jeolojisi. Cumhuriyet Üniversitesi, Yerbilimleri Dergisi (Seri A) 16, 95–106.

Yılmaz, Y., Yiğitbaş, E., 1990. The different ophiolitic metamorphic assemblages of SE Anatolia and their significance in the geological evolution of the region. Proceedings of the Eighth Petroleum Congress of Turkey. Turkish Association of Petroleum Geologists (TAPG), Ankara, pp. 128–140.